AD-A131 177 LATE TIME CONTAINMENT RESEARCH(U) S-CUBED LA JOLLA CA 1/1
R DUFF ET AL. 01 JUN 82 SSS-82-R-5396 DNA-TR-81-137
DNA001-81-C-0072

UNCLASSIFIED F/G 18/3 NL

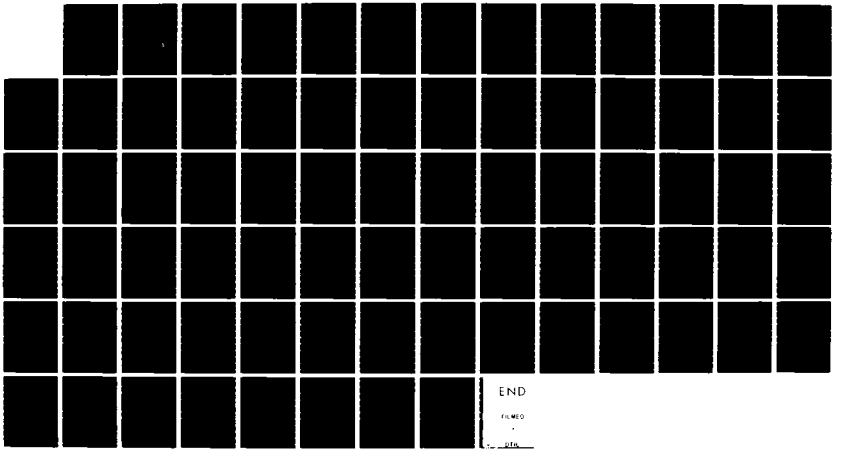

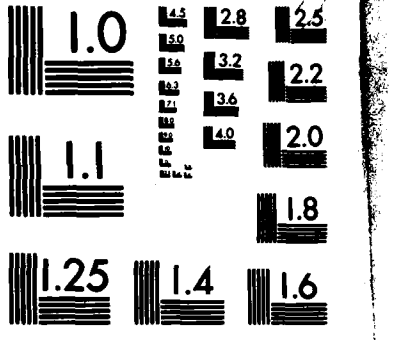

(12)

DNA-TR-81-137

LATE TIME CONTAINMENT RESEARCH

R. E. Duff
J. R. Barthel
K. Lie
W. J. Proffer
N. Rimer
S-CUBED
P.O. Box 1620
La Jolla, California 92038

1 June 1982

Technical Report

CONTRACT No. DNA 001-81-C-0072

APPROVED FOR PUBLIC RELEASE;
DISTRIBUTION UNLIMITED.

THIS WORK WAS SPONSORED BY THE DEFENSE NUCLEAR AGENCY
UNDER RDT&E RMSS CODE B345081466 J24AAXYX00010 H2590D.

Prepared for
Director
DEFENSE NUCLEAR AGENCY
Washington, DC 20305

Destroy this report when it is no longer needed. Do not return to sender.

PLEASE NOTIFY THE DEFENSE NUCLEAR AGENCY, ATTN: STTI, WASHINGTON, D.C. 20305, IF YOUR ADDRESS IS INCORRECT, IF YOU WISH TO BE DELETED FROM THE DISTRIBUTION LIST, OR IF THE ADDRESSEE IS NO LONGER EMPLOYED BY YOUR ORGANIZATION.

UNCLASSIFIED

SECURITY CLASSIFICATION OF THIS PAGE (When Data Entered)

REPORT DOCUMENTATION PAGE		READ INSTRUCTIONS BEFORE COMPLETING FORM
1. REPORT NUMBER DNA-TR-81-137	2. GOVT ACCESSION NO. AD-A131177	3. RECIPIENT'S CATALOG NUMBER
4. TITLE (and Subtitle) LATE TIME CONTAINMENT RESEARCH		5. TYPE OF REPORT & PERIOD COVERED Technical Report 6. PERFORMING ORG. REPORT NUMBER SSS-82-R-5396
7. AUTHOR(s) R. E. Duff, K. Lie J. R. Barthel, N. Rimer W. J. Proffer		8. CONTRACT OR GRANT NUMBER(s) DNA 001-81-C-0072
9. PERFORMING ORGANIZATION NAME AND ADDRESS S-CUBED P. O. Box 1620 La Jolla, CA 92038		10. PROGRAM ELEMENT, PROJECT, TASK AREA & WORK UNIT NUMBERS Task J24AAXYX-00010
11. CONTROLLING OFFICE NAME AND ADDRESS Director Defense Nuclear Agency Washington, D. C. 20305		12. REPORT DATE 1 June 1982 13. NUMBER OF PAGES 74
14. MONITORING AGENCY NAME & ADDRESS(if different from Controlling Office)		15. SECURITY CLASS. (of this report) UNCLASSIFIED 15a. DECLASSIFICATION/DOWNGRADING SCHEDULE N/A

16. DISTRIBUTION STATEMENT (of this Report)

Approved for public release; distribution unlimited.

17. DISTRIBUTION STATEMENT (of the abstract entered in Block 20, if different from Report)

18. SUPPLEMENTARY NOTES

This work was sponsored by the Defense Nuclear Agency under RDT&E RMSS Code B345081466 J24AAXYX00010 H2590D.

19. KEY WORDS (Continue on reverse side if necessary and identify by block number)

Red Hot	LOS flow
Misty Jade	Residual Stress
Diablo Hawk	Grout Spheres
Mighty Epic	Material models

20. ABSTRACT (Continue on reverse side if necessary and identify by block number)

This summary of Late-Time Containment Research describes the various tasks undertaken during 1981. Cavity conditions were estimated for Red Hot as a function of time, and consideration of connecting tunnel conditions suggested that venting from the cavity was energetically rather minor. Diablo Hawk diagnostic data permitted the identification of the second LOS flow pulse as steam at a temperature near 3500°K. The LOS flow in Miners Iron was found to have a pressure three times higher than on Diablo Hawk. LOS flow studies (over)

DD FORM 1 JAN 73 1473 EDITION OF 1 NOV 65 IS OBSOLETE

UNCLASSIFIED

SECURITY CLASSIFICATION OF THIS PAGE (When Data Entered)

20. ABSTRACT (Continued)

suggested that aerodynamic forces turn the helical insert into the flow and thereby intercept penetrating flow components. Particle velocity records from grout spheres tests were analyzed to show that the conventional material model for 2C4 grout is unacceptable. Probably strain rate effects, material damage and a relaxation time will be required to give agreement between calculations and the measurements. An algorithm was developed for use in the LANL KRAK code to improve calculations of crack propagation from a cylindrical borehole. This specified how pressure in the borehole should be treated. Several other tasks are discussed briefly.

TABLE OF CONTENTS

LIST OF ILLUSTRATIONS

SECTION 1
INTRODUCTION

This is the final report of activities undertaken during calendar year 1981 in the continuing support provided by S-CUBED to the Defense Nuclear Agency in the general area of Late Time Containment research. This work was supported by Contract No. DNA001-81-C-0072.

As in previous years an effort has been made during 1981 to report technical activities in a timely way in topical reports or in letters to interested parties. The presentation found here will, where appropriate, rely heavily upon these more complete discussions.

Contributions have been made in a number of areas. These include the analysis of past events and suggestions relevant to the design of future experiments, studies of line of sight of flow conditions, support for the LS experimental series conducted by Physics International, support for the grout spheres program conducted by SRI International and a number of miscellaneous activities. These items will be discussed in the following sections.

SECTION 2
TEST RELATED ACTIVITIES

Obviously a major responsibility of the Late Time Containment program is to provide design information, comment, and evaluation concerning specific nuclear tests which have been conducted or which are planned by DNA. Contributions in several such areas will be discussed below.

2.1 RED HOT/MISTY JADE

A major current effort in the DNA containment program involves the development of a containment scenario for a proposed cavity shot, Misty Jade, which is in many respects similar to Red Hot. As a result, an extensive program is underway to understand the Red Hot experience. It is generally believed that this understanding is a prerequisite to the development of a satisfactory containment prospectus for Misty Jade. The status of understanding of Red Hot phenomenology as of May, 1981, is summarized in a classified report entitled "Pressure Evolution Following a Nuclear Explosion in a Cavity". The Introduction, Summary and Conclusion section of that report are reproduced below.

"A nuclear explosion in a pre-mined hemispherical cavity, such as the Red Hot event and the proposed, very similar Misty Jade event, is of interest for the measurement of cratering effects. However, such an explosion is largely decoupled from the surrounding medium. As a result a large fraction of the yield remains in the cavity. This raises concerns about the satisfactory containment of the high pressure cavity gases.

"This report analyzes the evolution of cavity pressure as more and more of the surrounding rock is equilibrated with the cavity gas. This material may be mixed with the cavity gases, for example, as a result of ablation of crater ejecta during its flight through

the cavity or spallation of the cavity wall as a result of heat transfer from the cavity gases. The other major source of material for cavity quenching is chimney formation.

"The cavity pressures at various states of mass addition for Red Hot are estimated in Section 2. It is concluded that tens of thousands of tons of rock are required to get the cavity pressure down to safe levels (below overburden) for the yield and cavity volume considered. There is an intermediate regime where the pressure is highly "buffered" changing only moderately as the added rock mass increases from a few hundred tons to about ten thousand tons. The buffered level is estimated to be about 140 to 200 bars for Red Hot, assuming 20% moisture. The level is estimated at 80 to 110 bars for 10% moisture, suggesting a significant advantage in selecting a dry formation for any future cavity shot.

"The rates of removal of material from ejecta and from the cavity wall are considered in Section 3. It is concluded that ejecta ablation could not reduce the Red Hot cavity pressure to safe levels (below overburden) and that cavity wall spallation could do so only after a number of hours. The pressure is expected to be reduced to the buffered level within several seconds to several minutes.

"An inventory was made of the possible mechanisms whereby the cavity pressure may have been relieved in Red Hot. Although only limited information has been obtained by reentry work to date, it has been tentatively concluded that the energy vented into the access tunnel and Deep Well was insufficient to reduce cavity pressure significantly. The pressure may have been relieved by a crack opening into a porous medium above the cavity or by prompt chimney formation, or it may have been sufficiently reduced, by a combination of prompt ablation and the effect of relatively dry rock adjacent to the cavity, to enable the residual stress field to contain it. It is even possible that the residual stress field was sufficient to contain the pressure of perhaps

400 bars or so to which the cavity can rapidly drop by equilibrating the exposed sand and steel known to be present. This analysis is presented in Section 4.

"The implications of the Red Hot observations and the analysis contained in this report for Misty Jade are also discussed in Section 4. It is concluded that containment success for Misty Jade cannot be confidently predicted at this time. Containment prospects can be maximized by emplacing it in the driest medium possible without compromising its ability to produce a residual stress field.

"It should be stressed that this investigation has been carried out prior to a planned Red Hot reentry and is intended in part to provide guidance for that work. The findings of the reentry should enable us to narrow down the Red Hot scenario much more than is currently possible and to make predictions for Misty Jade with greater confidence."

In addition, a number of meetings and conversations have occurred in which a number of recommendations for the development of a productive reentry program have been presented to Field Command representatives. We continue to stand ready to assist with the analysis and interpretation of reentry observations as they become available.

2.2 DIABLO HAWK CONTAINMENT SUMMARY REPORT

The experimental data related to LOS flow conditions and late time gas pressure and composition have been collected, analyzed and interpreted in a classified Containment Summary Report for the Diablo Hawk event. Specifically this report describes the LOS plasma flow, the stemming motion, tunnel environment, residual stress and stress relaxation and the performance of associated tunnel systems.

The reverse cone used for Diablo Hawk was thinner than that used on Mighty Epic, and the iron vacuum vessel was outside of the tuballoy segments rather than inside of them. This design change was based on

calculational studies and problems which arose in the construction of the Mighty Epic system.

Many diagnostic measurements were made to determine the plasma characteristics in the LOS for this event. In general, good results were obtained, and the data provide the basis for an improved understanding of the flow phenomenology. Specifically, slifer, fluid coupled plate, and ported pressure systems were installed, and good data were obtained from most of them.

Relatively weak HMTW cable was used for slifer systems on Diablo Hawk. This cable has an estimated crush strength approximately one-half that of the standard cables used on Mighty Epic and previous events. These slifer systems clearly demonstrate that the plasma conditions on Diablo Hawk were more benign than in any previous experiment. The Brownlee knee was seen at a range of 28 m, and the data show strong evidence of a second plasma pulse arriving somewhat later. Qualitatively speaking, the second pulse was more prominant in Diablo Hawk than it was in Mighty Epic, but it is clearly evident in the slifer records from both events.

Fluid coupled plate and ported pressure gauges were installed between 70 and 110 m along the LOS pipe. All gauge systems provided data and confirm the two wave character of the plasma flow indicted by the slifers. The fast pulse has an apparent velocity of 1.3 cm/μs; the slower pulse a value of 0.42 cm/μs. In both cases the velocities are constant with range.

This diagnostic information was used to develop a flow scenario for the second pulse. It appears to have an incident pressure of approximately 0.2 MPA, a density of 1.2×10^{-4} gm, a sound speed of 0.15 cm/μs, and a temperature of 3500° K. The gas is thought to be largely steam generated from the collapsing grout near the end of the tuballoy reverse cone.

The calculated cavity formation and grout extrusion process suggested that stemming materials should have reached approximately 95 m from the working point. On the other hand, on reentry it was found that the DAC doors were completely shattered. Fragments were found throughout the region slightly before the DAC up to the MAC. A significant quantity of grout and three short sections of LOS pipe passed through the DAC opening. The DAC door fragments were heavily eroded by what appears to have been an extreme thermal environment. Fragments appeared to have been well "fried".

The relative motion of the grout at the LOS and at the tunnel walls was dramatically illustrated by the observation of about 20 m of displacement of LOS pipe sections near the DAC while essentially no relative motion occurred between tuff and grout at the tunnel wall in the same region.

Finally, chemical analysis of samples from the DAC/MAC area showed that fission fragments from uranium as well as many construction materials were present. The uranium came from the predicted jetting of the tuballoy cone, the fission debris was expected because of the neutron flux on the cone. The relative amounts of various isotopes observed were not characteristic of bomb debris. There was no evidence of any leakage from the cavity to the DAC region.

Pressure gauges had been installed in the doorwells of the DAC and MAC. Both provided information which indicates that the DAC doors failed at approximately 400 ms. It is speculated that the stagnated gases, primarily from the second pulse, were compressed by the oncoming grout column, and these gases provided the heat transfer medium which caused the observed erosion upon subsequent door failure.

Perhaps the observed grout extrusion 15 m beyond the point at which calculations had indicated extrusion would stop was related to the relatively large tunnel used in the Diablo Hawk compared to that of

Mighty Epic. True, the invert had been filled with tuff matching grout in an effort to make the configurations appear identical. Perhaps tuff matching grout does not behave quite like tuff under dynamic loads.

The late time pressure in the TAPS region reached a pressure of 24 psia 2.5 hours after Diablo Hawk, and it had decayed to ambient at the end of six days. In addition, gas chromatographic measurements were made on samples collected from behind the TAPS which indicated that the hydrogen concentration was 65% , CO concentration was 1% , oxygen and nitrogen totalled approximately 30%. Chemical arguments were presented based on the reactions of iron and water and iron and CO_2 which suggest that the temperature behind the DAC reached 4000-5000 K as gas was compressed by the oncoming grout column. Reactions with iron would have changed half of the water into hydrogen and simultaneously reacted most of the CO_2 present to CO.

Several conclusions can be drawn from the study of the late time tunnel environment. The first is that the observed explosive mixtures are normal for such events and they come quite naturally from the shock closure process, LOS pipe wall ablation, and known chemical reactions under reasonable thermodynamic conditions. The most important point is that these explosive gas components arise in processes occurring well removed from the cavity. The observations of explosive gases beyond the stemming of HLOS nuclear events at late time does not imply any cavity leakage into the tunnel system.

An effort was made to measure the residual stress through a hydrofracture system installed between 53 and 84 m of the working point. Only the system at 68.5 m was not heavily damaged during the event. It clearly shows a significant increase in fracture pressure within 5 minutes of the explosion. Subsequently it too failed. Nine days after the event the system damage was repaired, and hydrofracture measurements were then taken on all three systems. No significant residual stress was observed at that time. It is apparently true that a

significant residual stress was developed at the time of the explosion, but that some relaxation process had eliminated this stress within a nine day period.

2.3 MINERS IRON DIAGNOSTIC REVIEW

The Miners Iron diagnostic data available in the spring of 1981 was analyzed and compared with Diablo Hawk. This comparison is part of the effort required for the preparation of the Miners Iron containment summary report which will be written when the reentry has been completed. Several factors were evident in this comparison. The slifers again showed a clear Brownlee knee but it was at a range of 40 m compared to 28 m for Diablo Hawk. It was also apparent that muffler interactions with the first plasma pulse caused slifer signals which had not been seen heretofore. Fluid coupled plate and ported pressure gauges again provided particularly good data. Two pulses travelling with velocities quite similar to those of Diablo Hawk were again observed. The pressure amplitudes, however, were approximately a factor of three larger than those seen on Diablo Hawk, but they were still slightly below the average experience as determined by Sandia measurements.

In this case the expectation was that grout extrusion would destroy the closest closure at 98 m. Reentry shows that door survived.

Unexpectedly high pressures were observed in front of and between the closures and in front of the TAPS within a few minutes after Miners Iron. Pressures as high as 300-500 psi are estimated to have existed throughout these regions within the first hour after the event. Unfortunately no late time pressure or temperature information is available, and no gas quality measurements comparable to those from Diablo Hawk and previous events are available from Miners Iron. As a result, it will be impossible to discuss the chemical implications of the late time pressure environment in the MAC/TAPS region on Miners Iron in satisfactory detail.

2.4 HURON LANDING EXPERIMENTAL RECOMMENDATIONS

A number of recommendations were made for diagnostic systems to be included in the Huron Landing event. Specifically, it was suggested that slifers employ HMTW cable as in Miners Iron and Diablo Hawk and that at least one slifer be installed quite close to the LOS pipe to better indicate flow conditions within the LOS.

Huron Landing is the first HLOS event to include a helical insert to attenuate plasma and penetrating debris. It was recommended that particular efforts be made to install fluid coupled plate systems near 45 m to diagnose the performance of this new feature. Gauges should be located between and under the segments themselves. Special care should be taken to avoid electrical noise and to allow for relatively non-uniform pipe expansion.

It would be well to devise some kind of door impact monitor, if possible, and to install MAC doorwell pressure monitors of the sort used on Diablo Hawk. These might provide interesting data about the late time LOS pressure and the time of failure of the doors if grout impact were to occur.

Finally, special efforts were recommended to obtain good gas quality measurements and late time pressure and temperature indications for Huron Landing. The Diablo Hawk data suggested the chemical mechanism in which H_2/H_2O and CO/CO_2 ratios are particularly significant. We hope that gas samples can be taken and subsequently analyzed to provide comparable data from Huron Landing.

2.5 ADDITIONAL SUGGESTIONS

Additional rather short and informal analyses were made for the Huron Landing/Diamond Ace configuration which were reported to the COR through correspondence. Specifically, investigations were made of the

possiblity of using high explosive detonation products in the vicinity of the muffler to slow down the first plasma pulse enough to insure its capture by the DAC systems. It appeared that this could be accomplished if approximately 19 kg of explosive were detonated in the muffler region.

Consideration was given to the possibility of constructing the Diamond Ace LOS pipe from nested segments of cylindrical pipe, each segment of which would be a stock pipe size. An apparently attractive scheme for constructing a pipe and providing helical inserts was proposed.

SECTION 3
ANALYSIS OF JETTING SIMULATION EXPERIMENTS

This section presents a brief abstract of work which has already appeared in a detailed topical report (Ref. 2) prepared during the contract period as well as some additional results and insights obtained after the release of that report.

3.1 REVIEW OF WORK APPEARING IN TOPICAL REPORT

The report (Ref. 1) describes calculational and analytical studies of high explosive jetting experiments designed to simulate energy injection into a nuclear line-of-sight. Numerous experiments were performed by Physics International Co. (Ref. 2) using identical spherical HE sources embedded in wet sand. Damage was assessed by comparing the volume and depth of holes produced in aluminum target plates at the end of each pipe. An evacuated steel pipe, 19 mm o.d. and 0.3 mm thick, was the standard configuration. Many variations were used.

Axially symmetric experiments produced some unexpected results, for example: use of a 2 mm jacket of lead around a standard pipe produced holes about twice as great in depth and volume as the average of the standard configurations; use of an air-filled pipe with wall thickness of 0.7 mm produced triple the standard hole size. Two dimensional calculations for the Standard and Lead Wrap cases which did not include the thin pipe wall were totally inconsistent with these results. Calculations including the wall were quite consistent with the data if relative calculated energy in the particulate jet of wall material formed on collapse is compared with relative measured hole volume. In terms of absolute comparison, the calculated results are consistent only if the cratering efficiency of the shower of particulate matter is assumed to be three to five times smaller than that of a single particle at the same velocity - which is considered reasonable.

Simplified calculations including the wall were performed for all three axisymmetric configurations in the frame of reference of a steady shock to provide guidance for the calculations of the actual configurations with a decaying shock. These produced the unexpected result that all three jet particulate mass and energy at equal rates as a steady state is approached. This result is explained by an adaptation of impulsive jetting theory. The steady state results put constraints on explanations of the laboratory results. The stronger jetting in the Lead Wrap case, compared with the Standard, is attributed to slower response of the region of the source of the jet to decay in the driving pressure in the wet sand - the Lead Wrap configuration is better tamped. The 0.7 mm air filled pipe result is explained analogously.

Configurations employing helical spiral asymmetries, 0.3 to 0.5 mm thick, also produced unexpected results. Spirals resting against the outer pipe wall resulted in essentially no change in target damage, whereas spirals resting against the inner wall virtually eliminated target damage. As a consequence, original intuition that the spiral would prevent cratering because of inertial effects was abandoned. A postulated mechanism attributing the spiral effect to turning of the unattached spiral into the pipe by the action of the faster-arriving vapor flow (generated by energetic pipe implosion near the source) is presented in detail. This mechanism is shown to be consistent with all data acquired so far in the series of experiments. (Note added in proof: So-called scoping tests fired after this report was written do not show the postulated turning of the helix into the flow. Rather, flash X-ray photographs seem to show a catastrophic interaction between the helix and unobservable particulates which is accompanied by significant conversion of kinetic into internal energy.)

3.2 FURTHER ANALYSIS OF JETTING PHENOMENA

The scenario emerging from the work in Ref. 1 envisions shock-driven pipe collapse as the source of a jet of condensate or particulate material. This jet, which comes from the steel liners, forms the observed hole in the target plate by a process akin to hypervelocity impact cratering. The jet consists of a large number of small particles or droplets; interference between these causes the

"cratering efficiency" to be several times smaller than that observed with single incident hypervelocity projectiles.

Some of the collapsing liner is vaporized, especially at the higher driving pressures near the source. This vapor is thought to contribute little to the target damage. As noted above, it is also thought (by us at least) to be responsible for the turning of internal spiral helices into the path of the particulate jet, eliminating target damage almost entirely.

More recent efforts have given increased support to the above scenario. These include a quasi-analytic study of phase change of the collapsing liners and a review of the implications of data from the more recent LS-5 experiment by Physics International (PI), Ref. 3d. We now describe these.

The collapse of a liner (pipe wall) driven by a shock propagating parallel to the pipe axis in the surrounding medium has been treated by an approximate theoretical model presented in Appendix A of Ref. 1. The model is an adaptation of the theory of Birkhoff, et al (Refs. 3,4) which describes steady state jetting of a liner driven impulsively by a layer of high explosive. The present analysis considers a liner collapse driven by the pressure field behind a constant-velocity shock wave (Figure 3.1). The point from which the jet emanates is a stagnation point in the frame of reference of the shock wave. The quasi-steady analysis shows that the stagnation enthalpy is approximately

$$h_s \simeq \frac{u_\ell^2}{2} \tag{3.1}$$

where u_ℓ is the shock velocity in the frame of reference of the undisturbed medium. The analysis holds only for a constant shock velocity (steady flow in the shock frame), but Equation 3.1 should be a reasonable approximation when the shock speed decays gradually, as in the spherical-source experiments of PI.

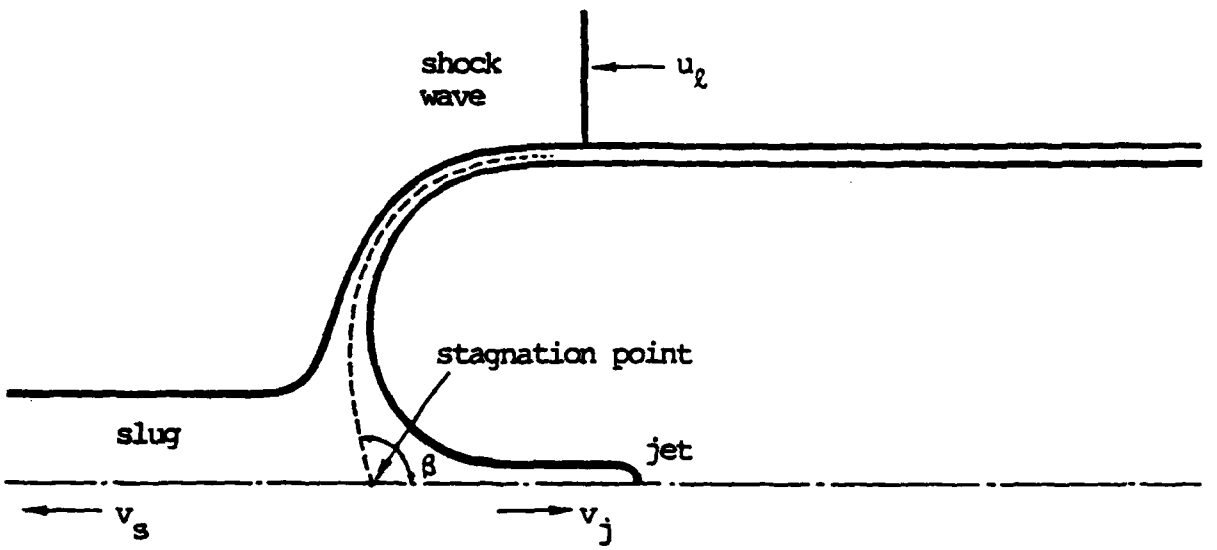

Figure 3.1. Steady shock-driven jetting configuration.

Condensate jetting should occur as long as h_s is sufficient to melt some of the wall material: i.e., $h_s \geq 2$KJ/g, or $u_\ell \geq 2$km/sec, for steel liners. This is not to say that the jet will remain liquid. The jetting material cools as it flows into the jet and is likely to become small solid particles. However, when h_s is insufficient to cause melting, the "incompressible fluid" analysis on which Equation 3.1 is based no longer holds because the material retains considerable strength in the plastic state. This suggests that the jetting process will probably cease, or greatly diminish, when u_ℓ drops below about 2 km/sec.

The above hypothesis can be compared with experimental results. Figure 3.2 shows the trajectories of the ground shock, the condensate jet, and the vapor arrival (data from Ref. 2). A reference line at 2 km/sec is also shown for comparison. The ground shock velocity drops below this value at an axial position of about 90 cm (60 cm from the HE source). In the simplified model the velocity of the collapse point (stagnation point) is equated with the ground shock velocity; for the actual decaying shock, the collapse point will start to lag the ground shock increasingly in the later stages of collapse. It is concluded that particulate jetting should end at about 60 cm from the HE, or a little less.

PI experiments have provided considerable insight into the length of the source of the penetrating jet. Use of "standoff" regions of wet sand, 10 to 50 cm in length, between the HE and the beginning of the pipe resulted in steadily diminishing damage to the target. As shown in Figure 3.3, the extrapolation of the results predicts "zero damage" at about 60 cm standoff. Other experiments using full length pipes with internal helical spirals extending from the HE only for part of the pipe length (to suppress the close-in jet source, as in the standoff cases) produced results consistent with the standoff results (Fig. 3.3). Thus the experimental results are consistent with the view that the penetrating jet is formed by melting of wall material on collapse.

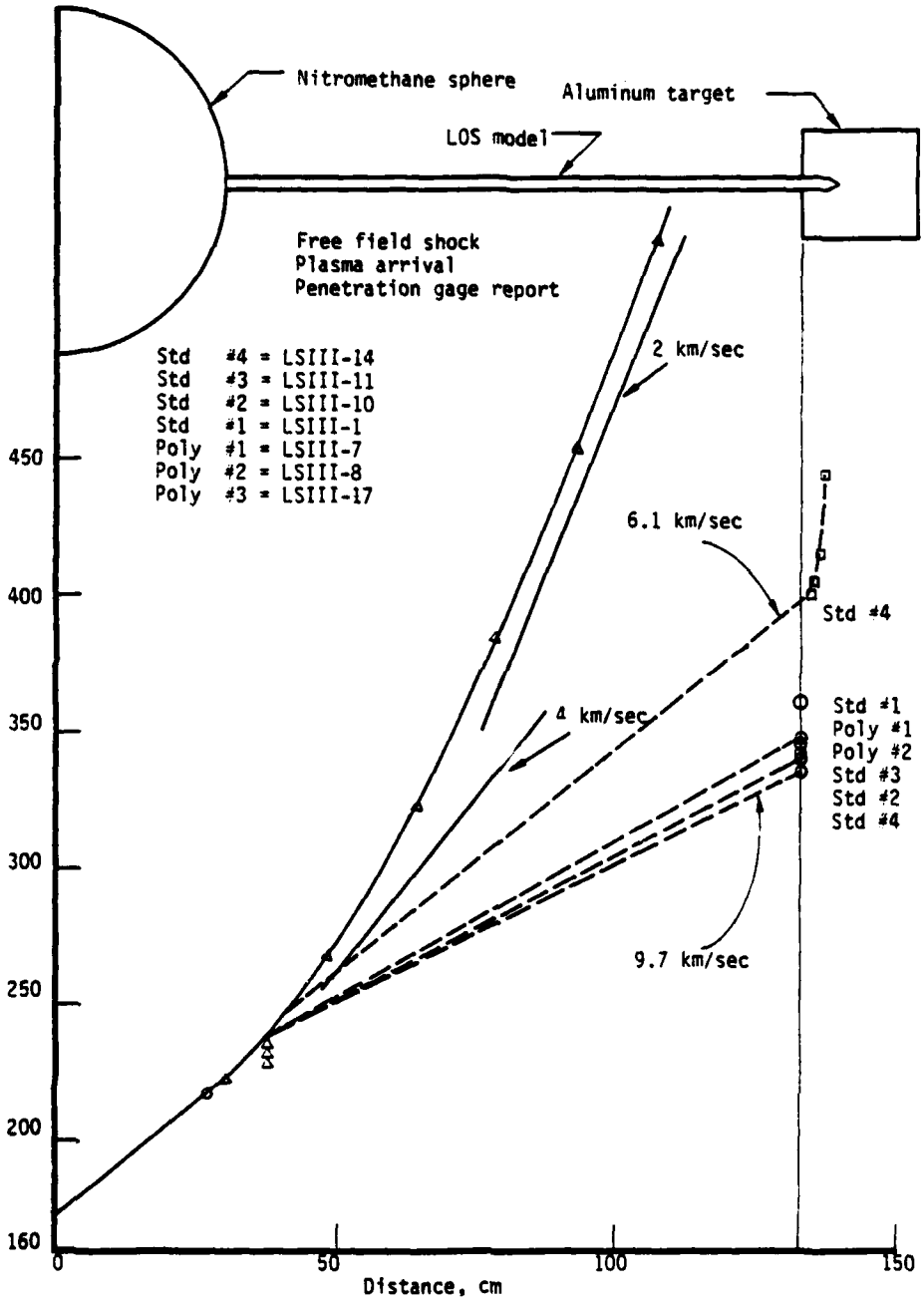

Figure 3.2. Arrival and penetration data from Standard and Polyolefin spiral configurations of LS III.

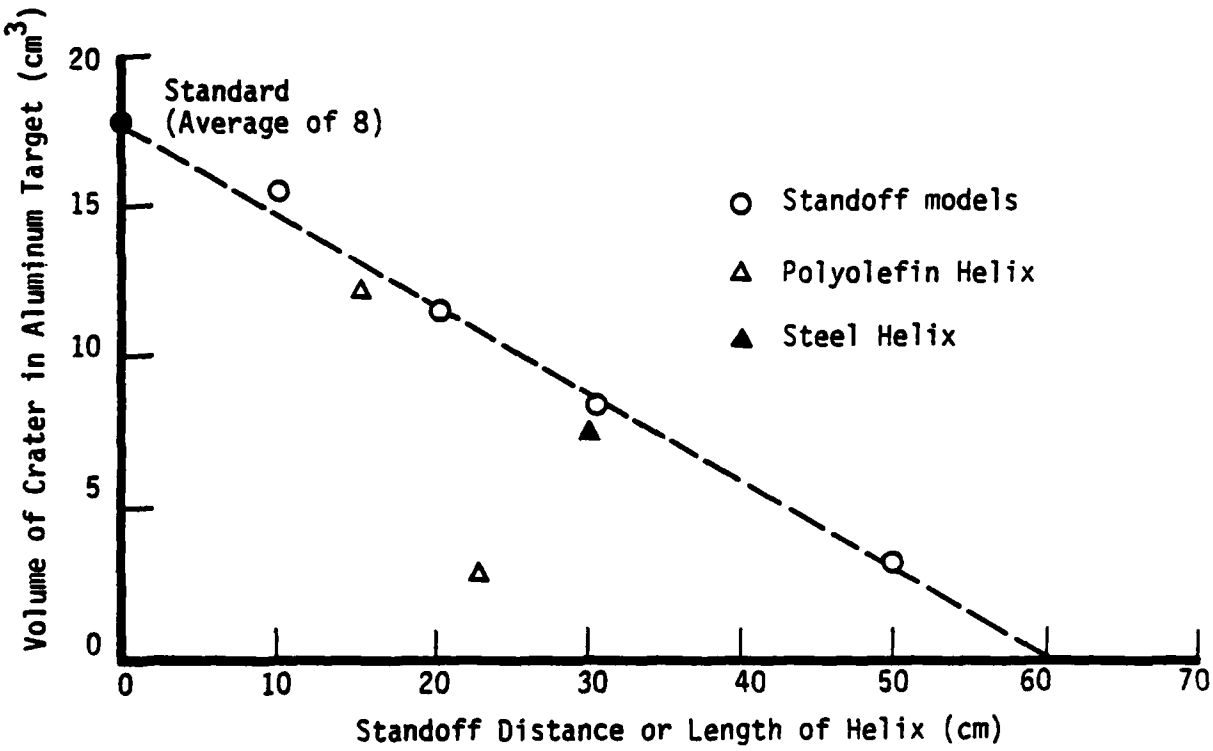

Figure 3.3. PI Data for Short Helix and Standoff Configurations.

At a stagnation enthalpy somewhat higher than the melt level one expects the pipe wall to vaporize at least partially. The ground shock velocity of 4.2 km/sec near the source should produce a stagnation enthalpy of about 8.8 KJ/g according to the steady state theory. Even larger transient values are seen in the full 2D calculation at the onset of pipe collapse. At the stagnation point, pressures of many hundreds of kbars are experienced which are well above the critical pressure of iron (thought to be in the range of 10 to 20 kbars). The distinction between liquid and vapor is meaningless above the critical pressure. However, pressures well below critical occur just ahead of the stagnation point (according to the calculations) and partial vaporization in the jet is expected for enthalpies of 3 to 4 KJ/g or more in this region. Calculations and data show that vapor is a significant component of the jetting material.

The above arguments suggest that the increased target damage observed in the PI Lead-Wrap case is due in part to a reduction of the vapor fraction in the jetting material. The calculated total energies for the jetting vapor plus condensates were nearly identical for the two cases.

Since the penetrating material is liquid or solid, but plenty of vapor is also formed, the question arises how target damage might change as the enthalpies of phase change are varied. At first glance, it would seem desirable to seek a material with a higher heat of fusion. However, this normally implies a higher heat of vaporization, and some energetic vapor generated close in would be replaced with condensates. This looks like a way of exchanging lower velocity particulates for higher velocity particulates, which is the wrong way to go. If, instead, one seeks a lower energy of vaporization, the question is whether the formation of more vapor comes at the expense of condensates, rather than as an increase of the total jetting. An adverse effect is expected to occur: material that is easily vaporized tends to be easily melted as well, and the condensate jet formation might then continue to considerably lower velocity of the collapse

point. But the associated specific energy ("penetrating power" per unit mass) would also diminish in proportion to u_ℓ^2. In effect, then, the use of wall materials with lower heats of phase change could reduce target damage unless the reduction of specific particulate energy is offset by a proportionate increase in mass of jetting particulates. This question deserves careful investigation from both the calculational and experimental point of view.

The practical implication of the above hypothesis is that it may be just as useful to reduce the fraction of jetting energy in condensed states as to reduce the total jetting energy. Even more intriguing is the fact that the postulated mechanism for the successful operation of internal spiral helices - turning of the helix into the path of the particulate jet by the vapor flow - would imply the same thing. If the jet is initially all vapor and the condensate jet begins later and at lower speed, there is more time for the mechanism to work. On tapered pipes this could become crucial (LS-5 showed that helical spirals become less effective as the taper increases).

The scenario for helix operation, while still tentative, has been made more credible by the results of the LS-5 experiment which was performed after the publication of Ref. 1. It was found that loose spirals are more effective than attached spirals. It was also found that the helix is more effective than a series of rings. In terms of the aerodynamic turning scenario, it would be expected that the turning, once begun, would be propagated along the pipe more readily than new turning could be initiated at each ring.

In summary, a phenomenological description of the mechanisms of target damage by jetting and of the prevention of target damage by internal spiral helices has evolved. These are consistent with the growing body of LS data. The practical implications of these suggested mechanisms are extensive. It is important to obtain as much information as possible on LS-6 to permit a sufficient level of confidence in either these or alternative scenarios.

3.3 TAPERED PIPES

The LS-5 experiment by PI included tapered pipes with "nominal" LOS taper (0.375° half angle), twice nominal taper, and four times nominal taper. There were two pipes of each taper without a helix; various helical and internal ring arrangements were also used. The following table summarizes the results without helices and compares them with the standard model results.

TABLE 3.1. SUMMARY OF PI DATA, STANDARD VS TAPERED PIPES (Refs. 2a, b, c, d)

	No. of Samples	Mean Hole Volume (cc)
Standard (zero taper)	8	17.8 ± 8.3
Nominal Taper (0.375° half angle)	2	14.35 ± ? (11.0 and 17.7)
Twice Nominal Taper	2	17.55 ± ? (14.8 and 20.3)
Four Times Nominal Taper	2	18.8 ± ? (both 18.8)

A pre-shot calculation was carried out with the STREAK code for the 4 x nominal taper for comparison with the standard model calculation. Figure 3.4 shows the growth of energy in the particulate jet (E_j) with time for each; Figure 3.5 shows the total energy in particulates and vapor. Using the assumption that the hole volume in the target is proportional to E_j, as in Ref. 1, one's initial inclination would be to predict that the hole volume in the target would be more than three times as large in the 4 x nominal taper model as in the standard model. The data suggest that such a result is not credible for any realistic values of the uncertainty in hole volume.

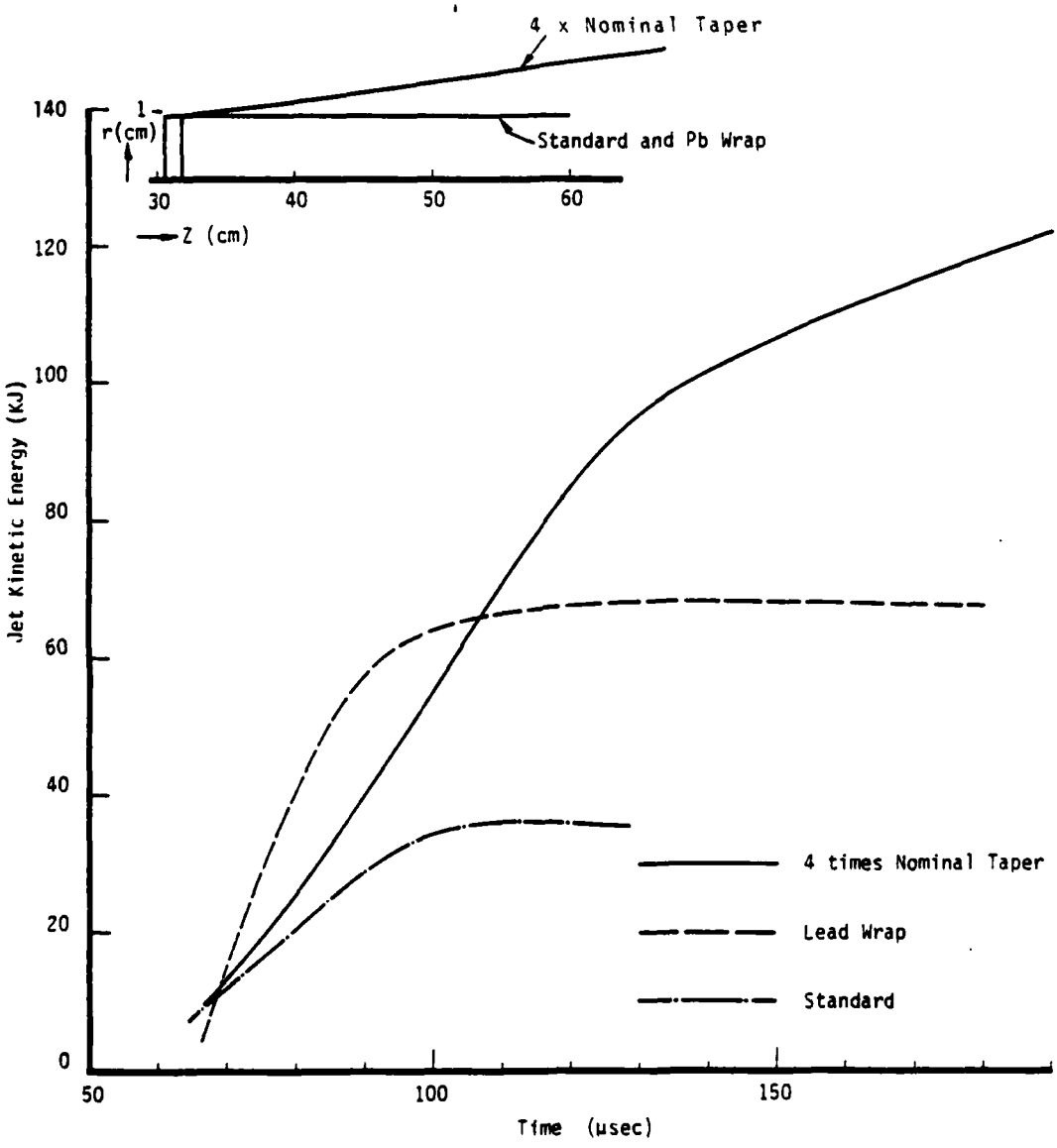

Figure 3.4. Growth of kinetic energy in the particulate jet.

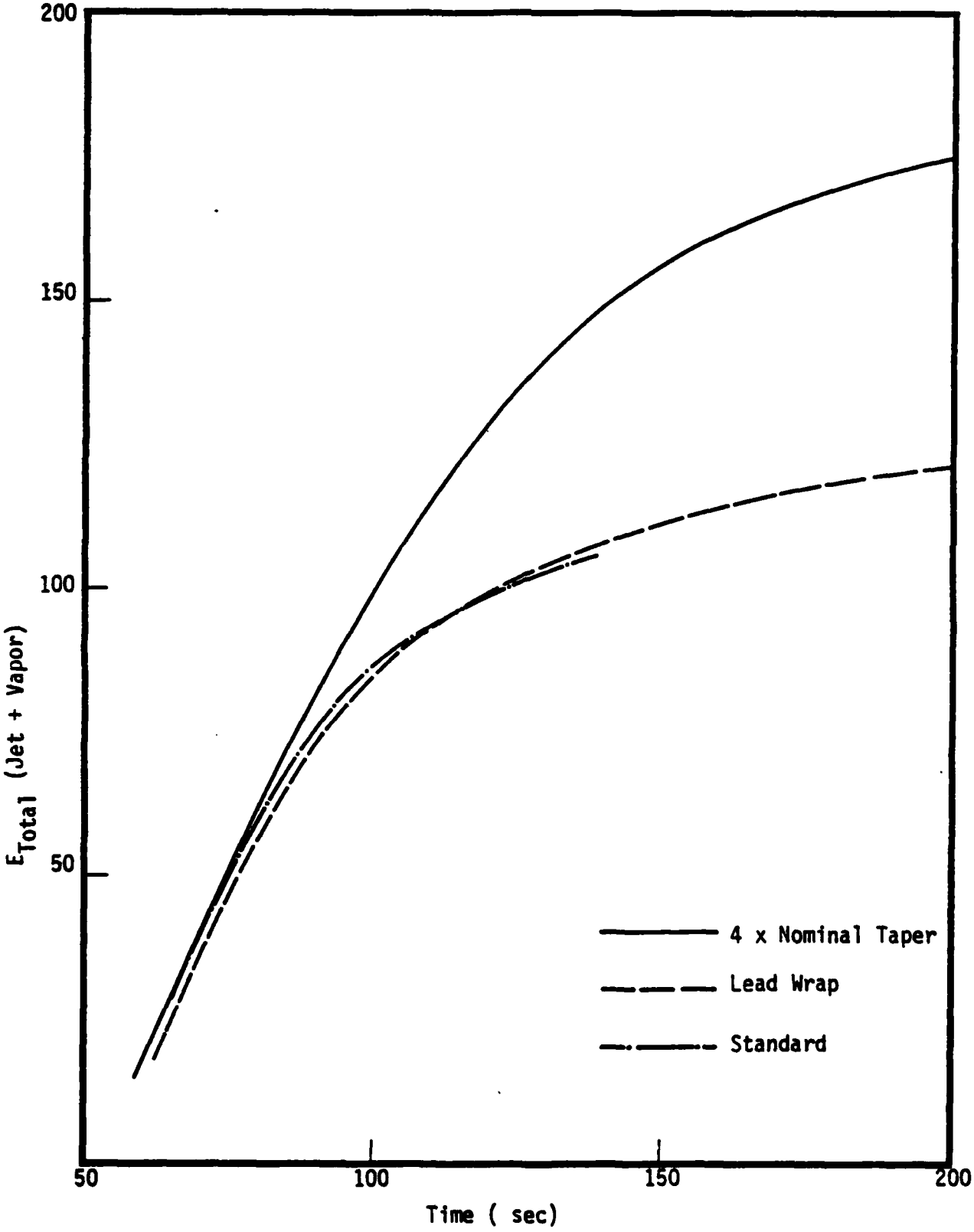

Figure 3.5. Growth of Total Energy (Particulate jet + vapor)

Further consideration of the calculational results provides useful insight. Notice that each calculation predicts a nearly-linear growth of E_j and E_{total} for a time, followed by a gradual decay of growth rate. The two calculations behave differently at late times. Energy continues to increase in the taper case but levels off in the standard. If the difference in the late stages can be attributed to numerics as discussed below, and the comparison is regarded as meaningful only in the rapid growth stage, the calculational comparison becomes much more consistent with the data.

Numerics can be critical at the stage where the particulate jetting is ending. These calculations using 0.9 mm radial zoning are, admittedly, marginally zoned for describing the jetting of collapsing 0.3 mm thick pipe walls (the fully-collapsed pipe extends 2.6 zones radially). Such zoning was necessary for economic reasons associated with the large ratio of pipe length to diameter. The comparison of the standard and Pb-Wrap calculations in Ref. 1 is meaningful only in a relative sense and only because precisely the same zoning was used in each. E_j stopped increasing in each after only about 20 cm of pipe was collapsed, whereas the actual source region of the jetting appears to extend to about 60 cm from the HE source. An intrinsic problem with the tapered pipe calculation is that the jetting source and collapsing pipe cannot both have exactly the same zonal resolution as in the standard model. The standard used 10 zones to describe the pipe radius. The taper calculation accomplished the same thing by using tapered zoning (this is a feature of STREAK's generalized coordinates); in this case, however, the collapsed pipe wall is resolved in fewer zones (its radius fully collapsed is proportional to the square root of its initial radius). If the taper of the zoning were selected to preserve the same resolution of the collapsed wall, then the pipe radius would be better resolved than in the standard.

Short of zoning both calculations more finely, all that can be done is to compare the rates of growth of E_j in the region before the particulate jet source becomes too weak to be sustained with the zonal resolution employed. The calculated ratio of tapered/standard E_j's is then interpreted, roughly, as 1.6 ± 0.3.

The above interpretation is not at all inconsistent with the data. There is an indication in the data of a trend toward increasing hole volume with increasing taper. Unfortunately, the results at zero taper do not fit this trend. However, note that the four standard models of LS-3 seem anomalously high (see Section 3.4). If the LS-3 results are due to some unknown inconsistency between the driving conditions in that experiment and the others, and therefore could be ignored, $\bar{V}$ would become 12.35 cc for the standard which fits the observed trend perfectly. This exercise would produce a ratio of $\bar{V}$ (4 x nominal taper)/$\bar{V}$ (standard) $\simeq 1.5$ which is totally consistent with the calculations.

Unfortunately, there is no substantial reason for ignoring the LS-3 standard results at this time. All that can be said is that the calculational results, prior to the rapid decay in energy growth, are not denied by the data because of significant uncertainty in $\bar{V}$ for the tapered pipes. It should also be pointed out that this revised interpretation of the calculations does not change the comparison of lead wrap vs standard (Ref. 1) because the slopes in the rapid growth stage in those calculations are proportional to the peak values of E_j.

One further comment about the calculational results. The calculations predict approximately equal total energy (vapor plus particulates) for the standard and taper cases but the taper case has less energy in vapor and more in particulates than the standard. This is qualitatively consistent with available time-of-arrival data for the vapor (ionization pins). The standard models (LS-2,3,4) indicated

vapor arrival velocities of about 0.85 to 1.2 cm/μs whereas the only tapered pipe (without helix) reporting data, twice normal taper, indicated 0.79 cm/μs (Ref. 2d). This is indicative that the vapor flow is less energetic in a tapered pipe.

3.4 STANDARD MODEL STATISTICS, REVISITED

Additional insights have been gained by reviewing the set of eight Standard model results for the hole volume in the target. First, it has been noticed that a lognormal distribution fits the data better than does a normal distribution. This is seen in Figure 3.6. This observation, previously overlooked, is completely consistent with the known tendency of quantities which cannot take negative values. (The normal distribution predicts that about 2% of Standard models will have negative hole volumes.)

It has also been noticed that the data spread is narrower if the eight samples of Table 3.2 are split into two distinct sets: the four samples from LS-3 and the other four from LS-2,4. The actual relative sample variance (S) is reduced even more by the separation into two samples (the "unbiased" standard deviation, σ, given by $\sigma^2 = S^2(N/N-1)$ for a sample of N results, is more inflated for smaller samples). The values of $S/\bar{V}$ are 0.31 for LS-3, 0.27 for the other four, and 0.44 for the combined eight. This suggests a likelihood that LS-3 was different from the others in some way. The shock trajectory in the wet sand was several percent faster in LS-3 than in LS-2 (Ref. 2c), which in itself doesn't seem a large enough effect to explain a factor of two in $\bar{V}$, but some related difference in the preparation of the medium or in the HE detonation may explain it. The separation of the standard experiments of LS-3 from those of LS-2,4 remains pure speculation, and even if it could be justified, it would not provide the much-desired justification for neglecting the LS-3 results in the analysis of the LS-5 tapered pipe results (Section 3.3): it seems the ground shock was just as fast in LS-5 as in LS-3 (Ref. 2d).

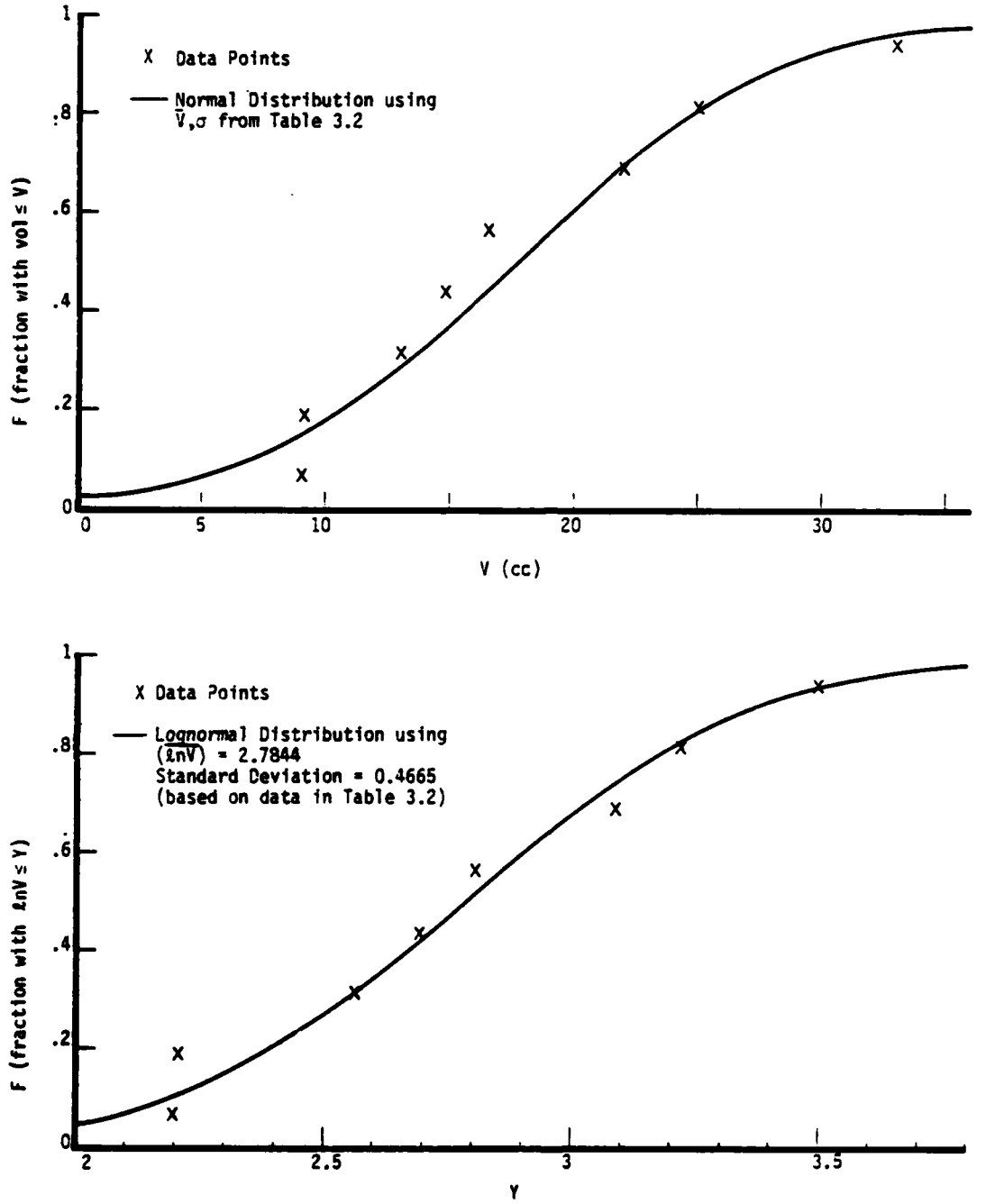

Figure 3.6. Comparison of Standard Configuration hole volume statistics with Normal and Lognormal distributions.

TABLE 3.2 SUMMARY OF TARGET HOLE VOLUMES, STANDARD MODEL

	Volume (cc)	$\bar{V}$(cc)	σ(cc)	$\sigma/\bar{V}$	$\bar{V}$	σ	$\sigma/\bar{V}$
LS3-1	13.0						
LS3-10	25.0						
		23.25	8.26	0.35			
LS3-11	33.0						
LS3-14	22.0						
					17.8	8.34	0.47
LS2-1	16.5						
LS2-2	9.1						
		12.35	3.87	0.31			
LS4-1	14.8						
LS4-2	9.0						

SECTION 4
LOS FLOW

This section discusses recent improvements in the phenomenological understanding of LOS flows and reviews the state-of-the-art in their calculational modeling (Section 4.1). It also discusses the implications of recent results for the optimization of closure design (Section 4.2). Some investigations carried out for specific shots are described in Section 4.3.

4.1 PHENOMENOLOGY AND MODELING

The two most recent horizontal LOS events, Diablo Hawk (DH) and Miners Iron (MI), produced LOS diagnostic data of a quality not previously achieved. Each of these events produced an internally consistent set of data at a number of stations along the LOS and the results of the two events were consistent with each other. This data base makes it possible, for the first time, to test hypotheses about the phenomenology of LOS flow.

The pressure history data from both events strongly indicate two distinct LOS pressure pulses at each station prior to ground shock arrival. This is seen in the examples given in Figures 4.1 and 4.2; data from all other stations show similar behavior. Figures 4.3 and 4.4 show peak pressure vs range for the first and second pulses, respectively, from DH and MI.* A striking feature of the results is the qualitative difference in the decay of pressure with range associated with the two pulses. The first pulse decays as R^{-3} whereas the second manifests an approximately exponential decay with range. (The upturn in the observed amplitude trends just before the MACs in Figure 4.4 is probably caused by the encounter with the detonation products and nitrogen released during the MAC actuation.)

* The data were provided by R. C. Bass and C. W. Cook of Sandia National Laboratories.

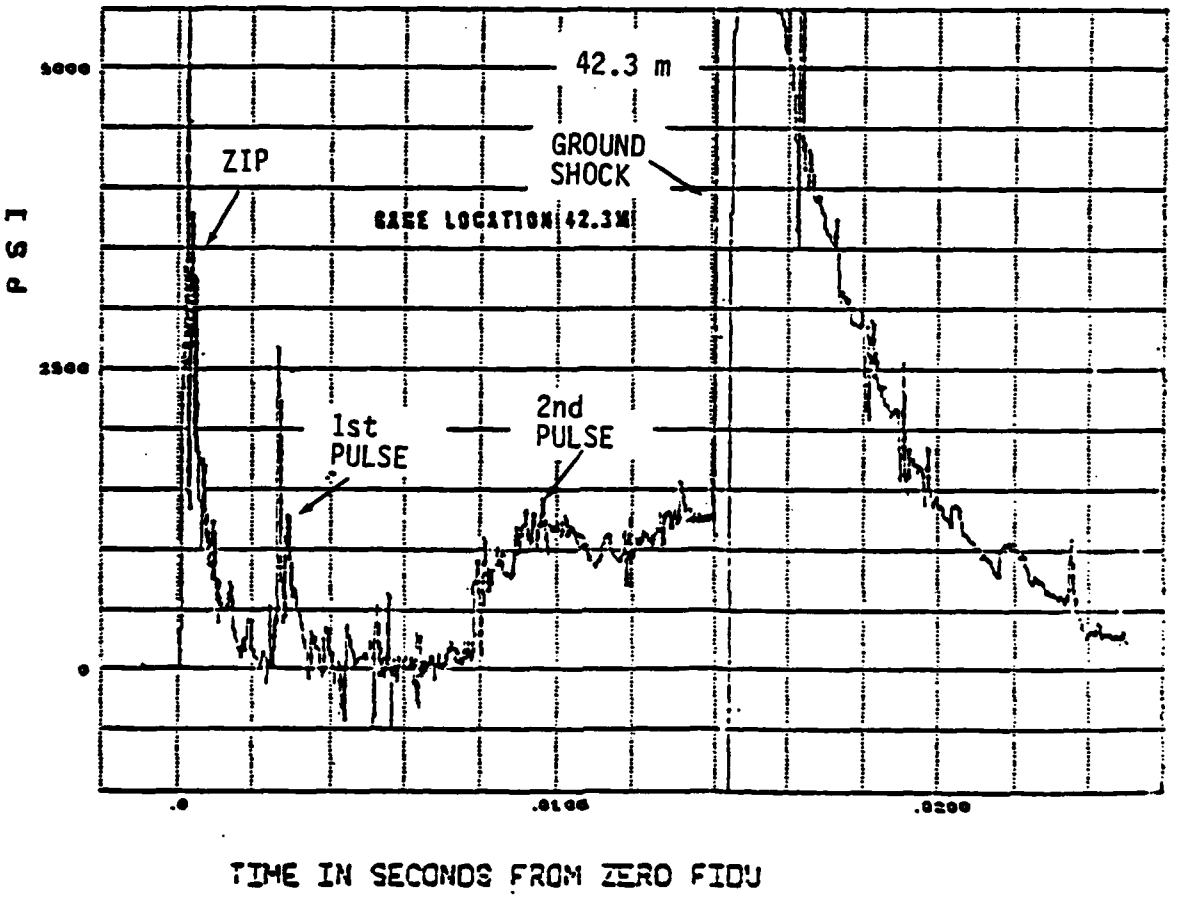

(145 psi = 1 MPa)

Figure 4.1. Typical LOS pressure history from Diablo Hawk.

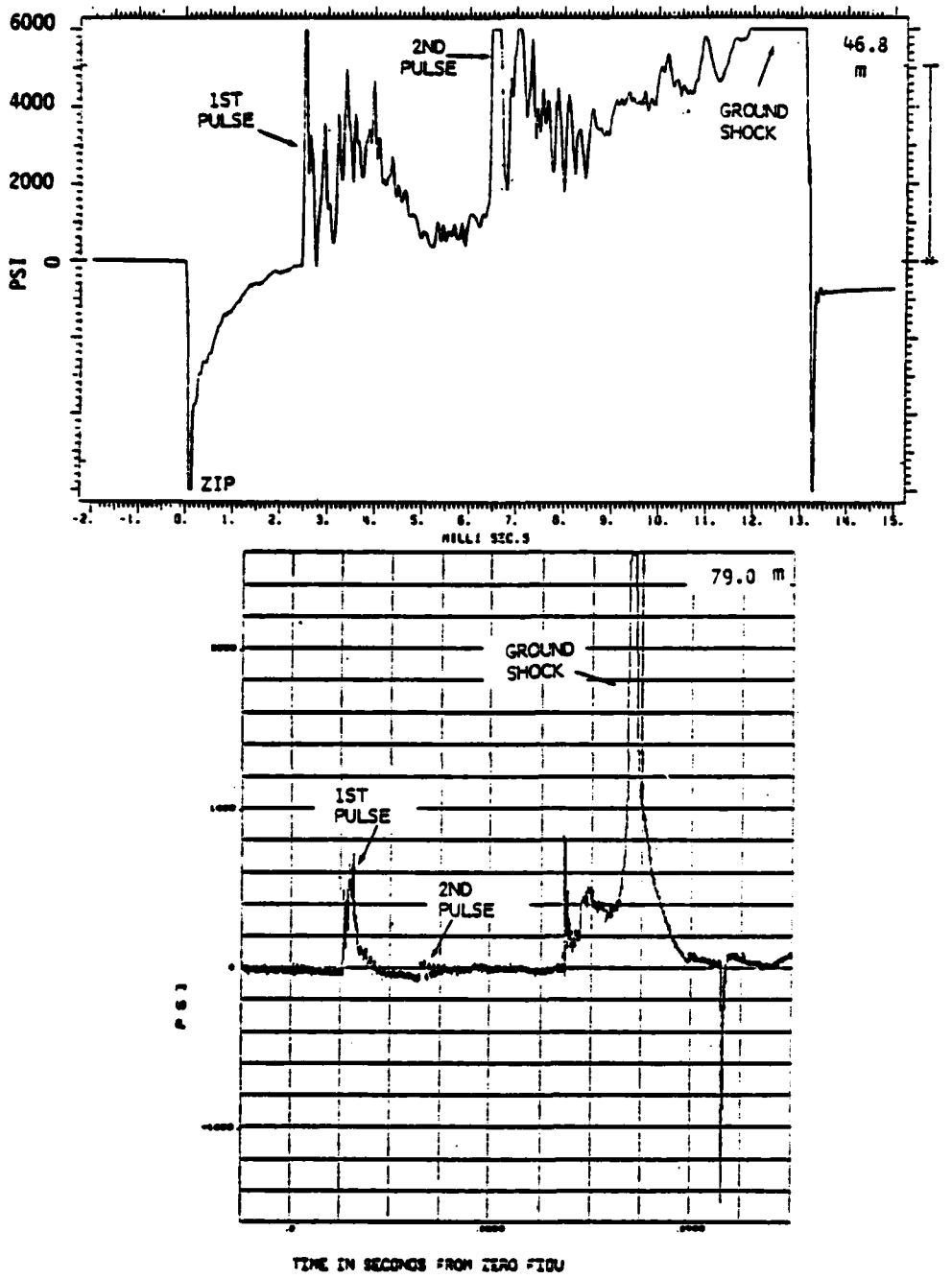

Figure 4.2. Typical LOS pressure histories from Miners Iron.

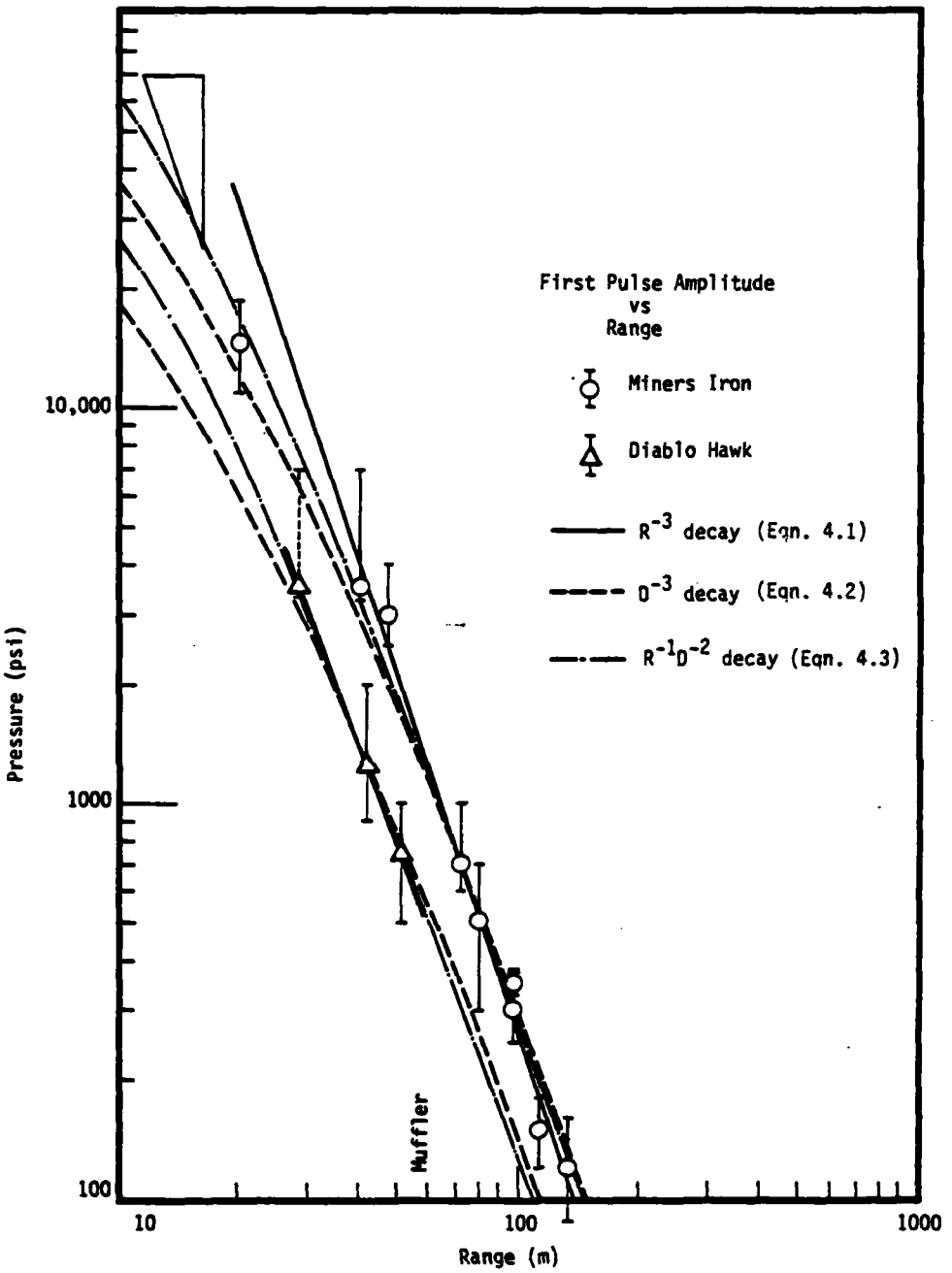

Figure 4.3. First pulse amplitude vs. range.

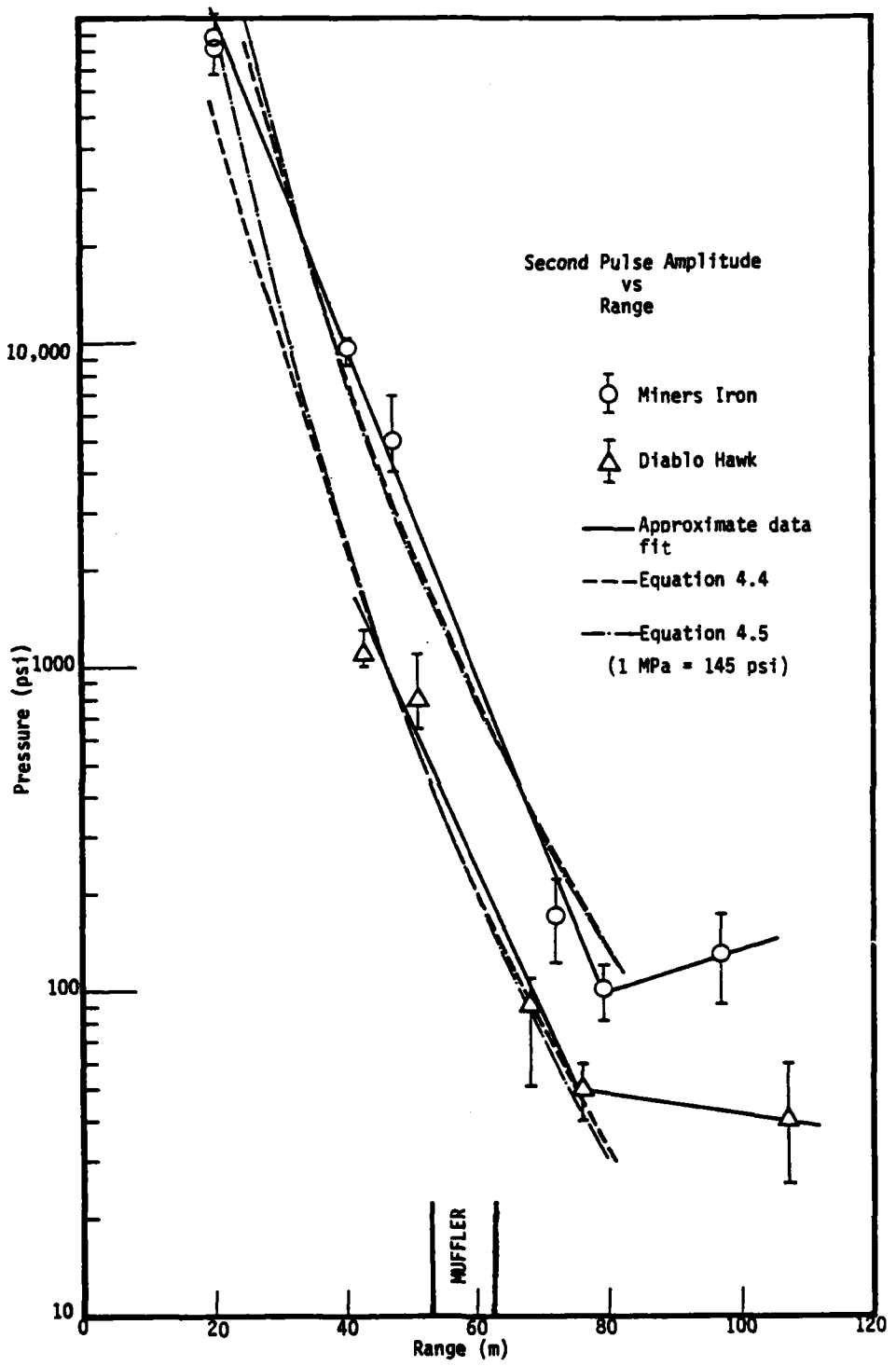

Figure 4.4. Second pulse amplitude vs. range.

These data challenge the analyst to provide phenomenological explanations. The rest of this Section is devoted to a presentation of such explanations and the reconciliation of calculations with the data.

Previous experience with LOS closure calculations provides ample evidence of two pulses. The first pulse is attributed to prompt energy injection into the LOS, primarily in the blowoff gases; this is formed by radiation-induced vaporization of the pipe wall and has no analog in the HE-driven simulations by PI. The second pulse is a consequence of further energy injection into the LOS by action of the ground shock; this is analogous to the vapor flow in the PI simulations with one important difference: in the simulations this pulse is an expansion into a vacuum whereas in the LOS it is a shock propagating into the residual gases of the first pulse. This probably explains the observed difference in velocity. The calculational comparisons presented later in this Section support this view.

The initial pressure associated with the blowoff gases decreases with range, and the associated pressure gradient rapidly initiates a flow in the pipe. The more dense blowoff gases nearer the source begin to expand into the near-vacuum farther from the source. The expansion is a combination of radial expansion resulting from the conical shape of the pipe and axial expansion along the pipe direction. Without significant wall interaction, this expansion would result in the one-way conversion of plasma internal energy into directed kinetic energy and an associated pressure drop. The pressure would decay as $V_{plasma}^{-\gamma}$, where V is the volume of a Lagrangian element of the blowoff plasma.

However, LOS flow calculations have always indicated much too early arrivals of pressure pulses along the axis unless ablation is considered. Ablation of the wall continually adds mass to the flow and dissipates kinetic energy. Calculations considering only the blowoff gases (discussed below) indicate that the partition between directed and internal energy remains nearly constant after an initial

transient behavior. That is, the dissipation and expansion effects offset each other. In this case, the pressure of an element should vary inversely as its volume:

$$p \propto v^{-1}$$

As the element moves to increasing range (R) its cross-section varies as R^{-2} because of the conical pipe and its axial length may be assumed to vary as $R^{-(1+\varepsilon)}$ where ε may be positive or negative and is thought to be small. This implies a decay of pressure with range of the form

$$dP/P \propto - 3dR/R,$$

$$P/P_o = (R/R_o)^{-3} \qquad (4.1)$$

which is consistant with the experimental data except at close range.

A refinement of the above approach takes into account the fact that the pipe diameter does not approach zero with R. One alternative formulation is

$$dP/P = - 3dD/D$$

where the pipe diameter, D, is given by

$$D = D_o + \alpha(R-R_o) .$$

R_o, D_o are the values at some reference point. Integration produces the following:

$$P/P_o = (D/D_o)^{-3} \qquad (4.2)$$

Another alternative, seemingly more defensible, superposes an axial expansion term, -dR/R, and a radial expansion term, -2dD/D, to obtain dP/P. The result of integration is:

$$P/P_o = (R/R_o)^{-1} (D/D_o)^{-2} \qquad (4.3)$$

The predictions of Eqs. (4.2) and (4.3) for decay of the first pulse are shown in Figure 4.3. (Each curve was fitted to the data at one point.) It is seen that both are superior to Eq. (4.1) for small R, with Eq. (4.3) slightly favored, whereas all three are equivalent at long range (where dD/D ≈ dR/R). The parameters used in producing the curves are shown in Table 4.1

TABLE 4.1. LOS PIPE PARAMETERS FOR DIABLO HAWK AND MINERS IRON

	DH	MI
α	0.01309	0.0144
R_o (m from WP)	11	11
D_o (m), at R_o	0.305	0.335

The second pulse is regarded as a shock wave because it propagates into the residual gas of the first pulse. Extensive experimental information on the decay of strong shock waves in straight pipes exists, e.g., the material summarized in Ref. (5) (both nuclear and HE driven). An exponential decay with range characterizes such shocks when the flow behind the shock is hot enough to ablate the wall:

$$P_s \propto \exp(-KR/D)$$

where K is a constant. $K \simeq 0.0576$ is consistent with most of the data, in particular, from the nuclear shock tube events, Hybla Gold and Marvel. The R/D dependence can be justified analytically. The observed end of the exponential decay regime is also consistent with the postulated ablation process. For shocks into ambient air, the exponential decay gives way to a more gradual decay at just the point where the post-shock air is no longer hot enough to vaporize the wall material ($P_s \sim 100$ to 300 bars). For shocks into a residual plasma, say iron vapor, ablation should play a role down to considerably lower pressures.

In a tapered pipe, it is proposed that the decay of shock pressure with range be expressed as a superposition of ablation-dominated shock decay as described above and of taper effects as in the analysis of the first pulse. The analog of Eq. (4.2) is obtained by setting

$$dP/P = - KdR/D - 3dD/D$$

Substitution of the pipe taper relation, followed by integration, produces

$$P/P_0 = (D/D_0)^{-(3+K/\alpha)} \qquad (4.4)$$

Alternatively, the analog of Eq. (4.3) is obtained in similar fashion:

$$P/P_0 = (R/R_0)^{-1} (D/D_0)^{-(2+K/\alpha)} \qquad (4.5)$$

The predictions of Eqs. (4.4) and (4.5) for the decay of the second pulse are shown in Figure 4.4. The predictions are generally quite consistent with the data. Eq. (4.4) appears better-behaved for small R; otherwise, it is difficult to choose between the two. (The analog of Eq. (4.1) behaves worse at small R and is not shown.)

The above exercise indicates that the physical assumptions on which it is based are reasonable: namely, that the first pulse is an expansion into a near-vacuum, the second pulse is a shock wave, and both are strongly influenced by ablation. There is some uncertainty as to details, but the qualitative behavior of all of the alternative expressions is reasonable. It is especially notewothy that the quasi-analytic expressions derived here are consistent with the experimental observation that the amplitude of the second pulse exceeds the first at short range but the opposite is true at long range.

The Diamond Ace event has been designed with a larger pipe taper than usual. Therefore, it constitutes a useful test of the validity of the above quasi-analytic techniques of as well as of calculational techniques for LOS flow. Investigations of the effect of LOS taper on second pulse decay, using Equations 4.4 and 4.5, have shown that although the term D in the argument grows more rapidly if α is increased, this is somewhat offset by the accompanying reduction of the exponent. That is, the ablation-dominated aspect of shock decay becomes less prominent with increased taper. Nevertheless, an increase of taper for fixed values of R, R_o, D_o and K does result in a reduction of P/P_o for all combinations likely to be interesting. We look forward to the comparison of Diamond Ace data with computational and quasi-analytic results.

A brief comment on muffler effects is in order. The muffler location is indicated in Figures 4.3 and 4.4 (approximately the same for both events). There is no indication of a change in the trend of pressure decay at the muffler. We interpret this as evidence that the muffler has little or no effect on flow amplitudes. However, R. C. Bass of SNLA interprets the data somewhat differently and believes the muffler has some effect.

A comparison of calculational predictions with the MI/DH data set is in order. The desired calculations would be STREAK calculations initiated from RAD9 calculations as early and as correctly as possible.

This is not quite what exists, as we shall see, but what exists is adequate for an assessment of how well the current calculational technique performs.

A preshot LOS flow calculation for Diablo Hawk was performed in 1976 with the UNION code. The FLIP segment then in use employed an ablation model that is now obsolete. The calculation was initiated at 0.1 ms from a RAD9 solution and carried to 4 ms. The primary purpose of that calculation (which was the last in the series performed as part of the DH closure design effort) was a comparison of predictions of injected plasma and particulate energy into the LOS with those predicted for other configurations. The secondary purpose was to make preshot LOS pressure history predictions to compare with the eventual data; for this purpose an LOS calculation was continued on stand-alone FLIP from 4 ms to more than 60 ms. The calculated arrivals proved to be quite late compared with the measurements.

Later, the ablation modeling was completely overhauled following Hybla Gold. The revised model was shown to give much better agreement with observed arrivals - at least to the muffler (see a classified report on LOS studies, 1981); the less rapid ablation obtained with the new model allowed faster arrivals. STREAK then replaced UNION as the primary 2D code for closure calculations. It employed the up-to-date ablation modeling for pipe flow. The DH closure calculation was repeated from 0.1 to 4 ms with STREAK in 1981. The LOS flow calculation after 4 ms was again continued with the stand-alone FLIP. Although the calculated plasma arrivals were much improved, they were still distinctly later than observed.

The results of the STREAK/FLIP calculation and the experimental data shown in Figure 4.5 for the 42.3 m station are typical. The calculated first pulse begins at about 4 ms whereas the observed first pulse begins at about 2.5 ms. The calculated second pulse begins at about 8.5 to 9 ms, less than 1 ms late - a much smaller percentage error in pulse speed than with the first pulse. Both calculated pulse amplitudes are too large by more than a factor of two.

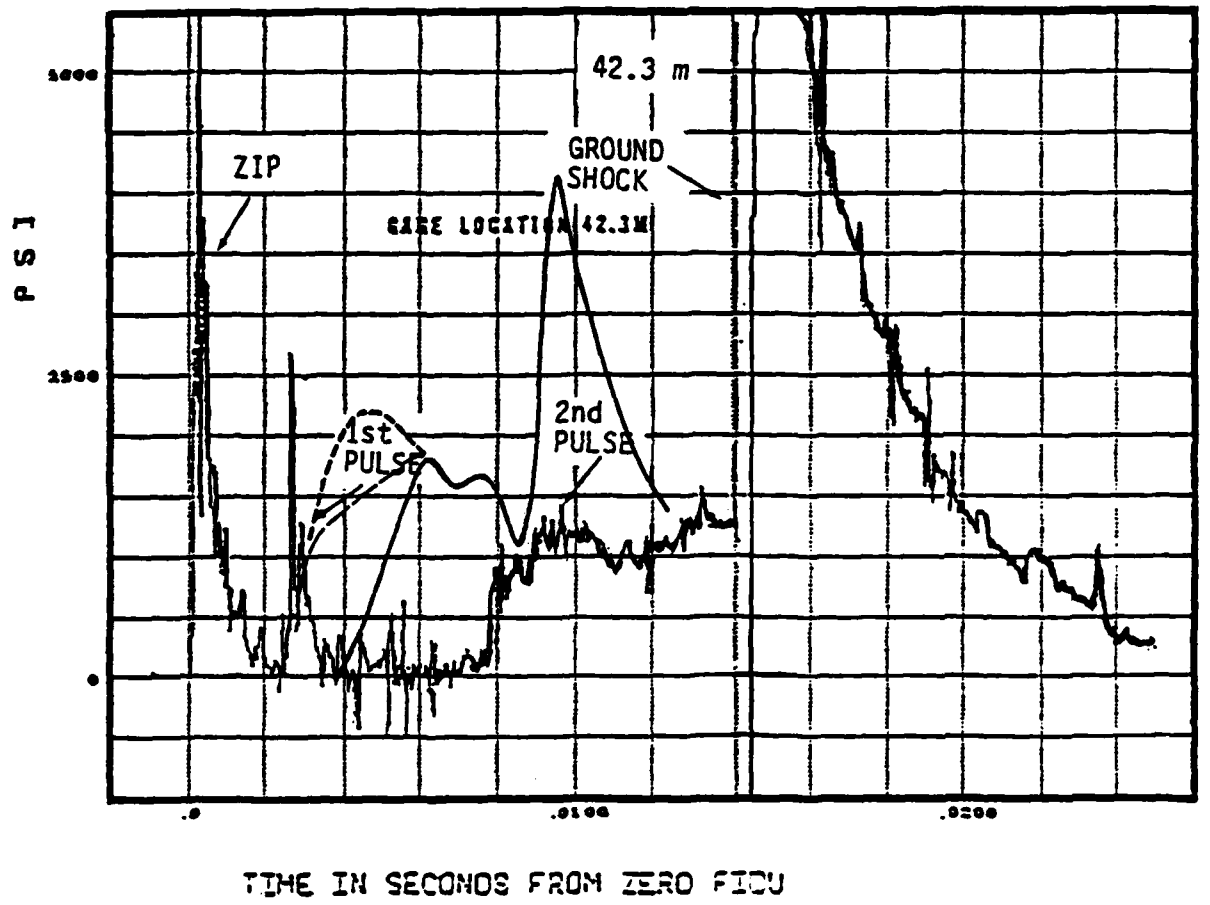

——— 2D STREAK to 4 ms, continued on FLIP (Quasi-1D, see Refs. 2,8)
Blowoff close-in only(see text)

– – – Blowoff only, FLIP

------ Expected result if full blowoff included in the full 2D calculation.

Figure 4.5. Calculated and measured LOS pressure histories from Diablo Hawk.

The reason for the discrepancy in the first pulse onset time was found to be in the treatment of the prompt blowoff vapor. The RAD9 calculation of the first 0.1 ms had included prompt blowoff only in the initial grid which extended a short distance beyond the zero room. As that calculation progressed and the spatial grid was expanded, the added sections of LOS were initiated with nominal low-density, low-pressure vapor conditions. This was of no real significance to the determination of LOS closure behavior or of energy injected into the LOS. However, it resulted in the loss from the calculation of significant initial blowoff vapor as well as additional LOS vapor which left the grid during each stage of calculational zoning.

We decided to initiate a FLIP calculation with a complete representation of the DH blowoff vapor. Although no additional energy injection was considered, this was expected to provide a fair representation of first pulse arrival. The comparison of the results with the first pulse onset data, Figure 4.6, supports this view completely. The wave form at 42.3 m from this calculation is shown in Figure 4.5; also shown is an estimate of how this first pulse would peak if it were determined in a full 2D calculation describing the continuing LOS energy injection process. The results indicate that the present calculational tools are highly credible as to their ability to predict two distinct LOS plasma pulses with appropriate arrival times. Further confirmation of this claim is given in the comparison of calculated and measured second pulse arrivals for DH (Figure 4.6). A blowoff-only calculation has also been performed for Miners Iron. The calculated arrival times are again in good agreement with observed first pulse arrivals, (Figure 4.6).

The calculated pressures in Figure 4.5 are 2 to 3 times too high. The same was found at other stations in Diablo Hawk. This chronic problem with LOS calculations is attributed to the inability of the

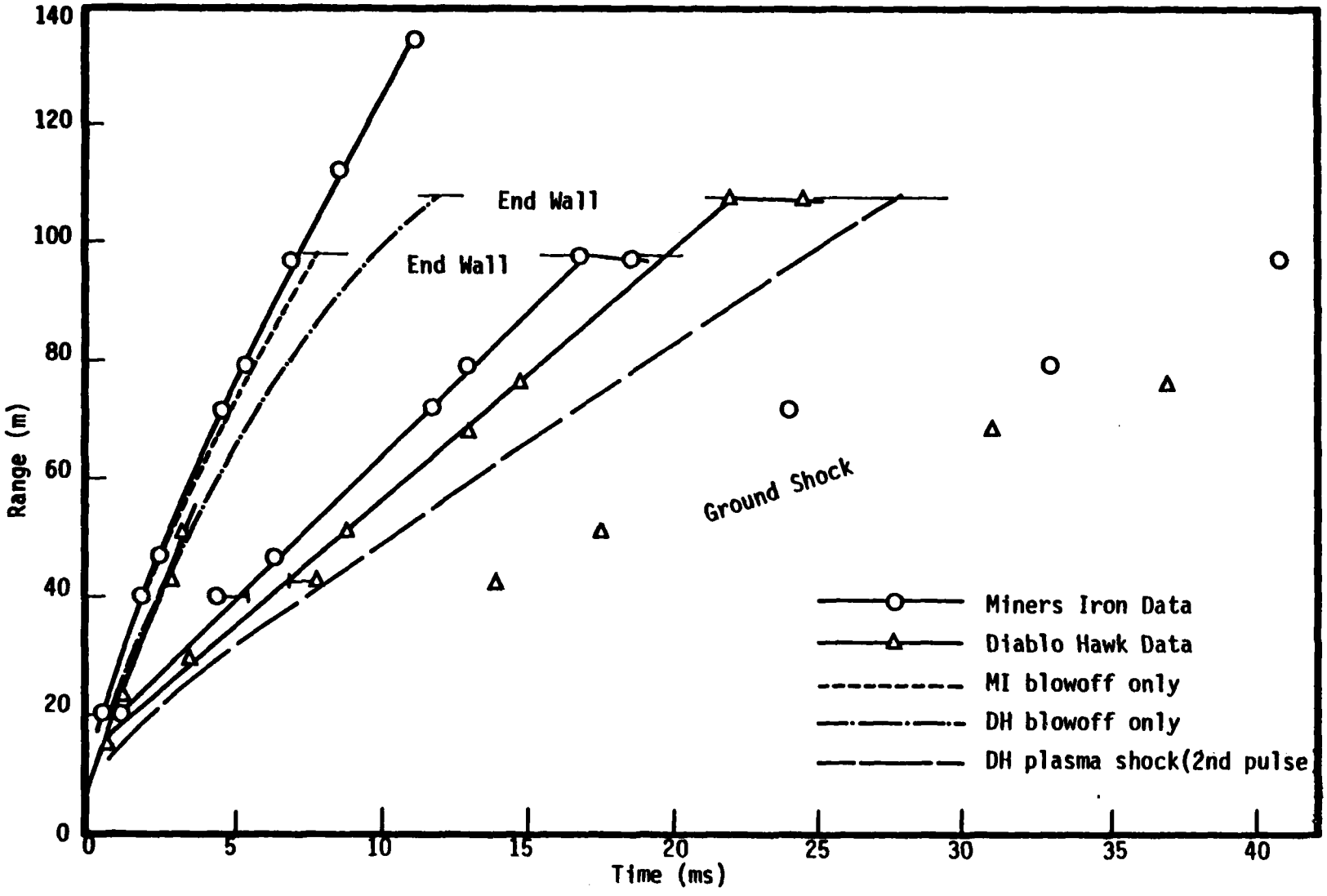

Figure 4.6. Comparison of measured and calculated pulse arrivals, Miners Iron and Diablo Hawk.

current modeling to treat quenching mechanisms such as massive entrainment of exposed grout after pipe rupture during expansion and loss of vapor into cracks and into the advancing ground shock-driven collapse region.

Despite this shortcoming, it is apparent that calculational techniques have improved substantially during the past several years. The ablation modeling enjoys growing credibility by virtue of calculational results that are consistent with a broad data base (see also the comparisons presented in Ref. (5)). Admittedly, the evidence for ablation is only indirect. However, other calculations have shown that when ablation is ignored in high-enthalpy flows, the calculated pressure pulses arrive much too early and have much too low amplitude. And it is especially compelling that the rate of attenuation of a shock propagating into an air-filled pipe has been observed to undergo a significant reduction at just the range where the air temperature behind the shock becomes too low to vaporize the wall (Hybla Gold 1 ft pipe, Ref. 5).

It is concluded that our calculational tools are steadily improving with the aid of a growing base of high quality data and a persistent effort to improve the physical modeling. These tools are quite credible as to their ability to predict two distinct LOS plasma pulses with reasonably accurate arrival times. The tendency to overestimate pressures is at least conservative and the reasons for it appear to be understood. To complete the analogy with the PI simulations, the 2D closure calculations for the LOS also indicate the formation of a jet of particulates. The leading edge of this is somewhat slower than the calculated second shock. There are insufficient experimental data for quantitative comparison with calculations, however, cratering of MAC/DAC doors has been observed in all cases where those doors have been recovered.

4.2 CLOSURE OPTIMIZATION

It is useful to review the position of closure design on its evolutionary path and consider what improvements might be realizable in the near future. We will consider: tuballoy extensions; helical wraps;

a proposed high explosive-driven closure FAC (fast-acting closure) similar to the super HE machine used on VLOS events; and stemming materials.

The development and evolution of tuballoy extensions over four DNA events has been the most recent major change in closure design. This evolved from a 1975 calculational study. There is strong evidence that their use has reduced the injection of energetic vapor into the LOS. This is demonstrated in Figure 4.7 which shows measured peak pressure (the larger of the first and second pulse) vs scaled range for a number of events, seven with iron extensions and three with tuballoy.* Even Miners Iron, which surprisingly produced peak pressures several times higher than Diablo Hawk (see also Figures 4.3 and 4.4), is seen to be quite benign in this context. The Miners Iron result is still under study, but the cause of the unexpectedly high pressures is thought to be the larger LOS diameter near the source, not the performance of the tuballoy extension.

The tuballoy extension reduces energy injection into the LOS because its high density slows the velocity of convergence of material toward the pipe axis. The role of a slower extension collapse in generating cratering flow must be carefully considered. As discussed in Section 3.2, the collapse of a steel liner at velocities between about 2 and 4 km/s should produce a predominantly condensate jet. The increased target damage in the PI lead wrap simulation may be due in part to the production of a jet that is less-fully vaporized. The optimization of the tuballoy extension must include careful analysis of this problem of vapor/condensate partition. The experience with PI simulations teaches that such analysis requires calculations which adequately resolve important features such as the steel liner inside the tuballoy. Such calculations were begun during the contract period but did not reach conclusive stages. These are continuing as part of the follow-on research effort.

---

* The data summarized in Figure 4.7 were provided mostly by R.C. Bass of Sandia, though some other sources were used and there has been some interpretation by the authors.

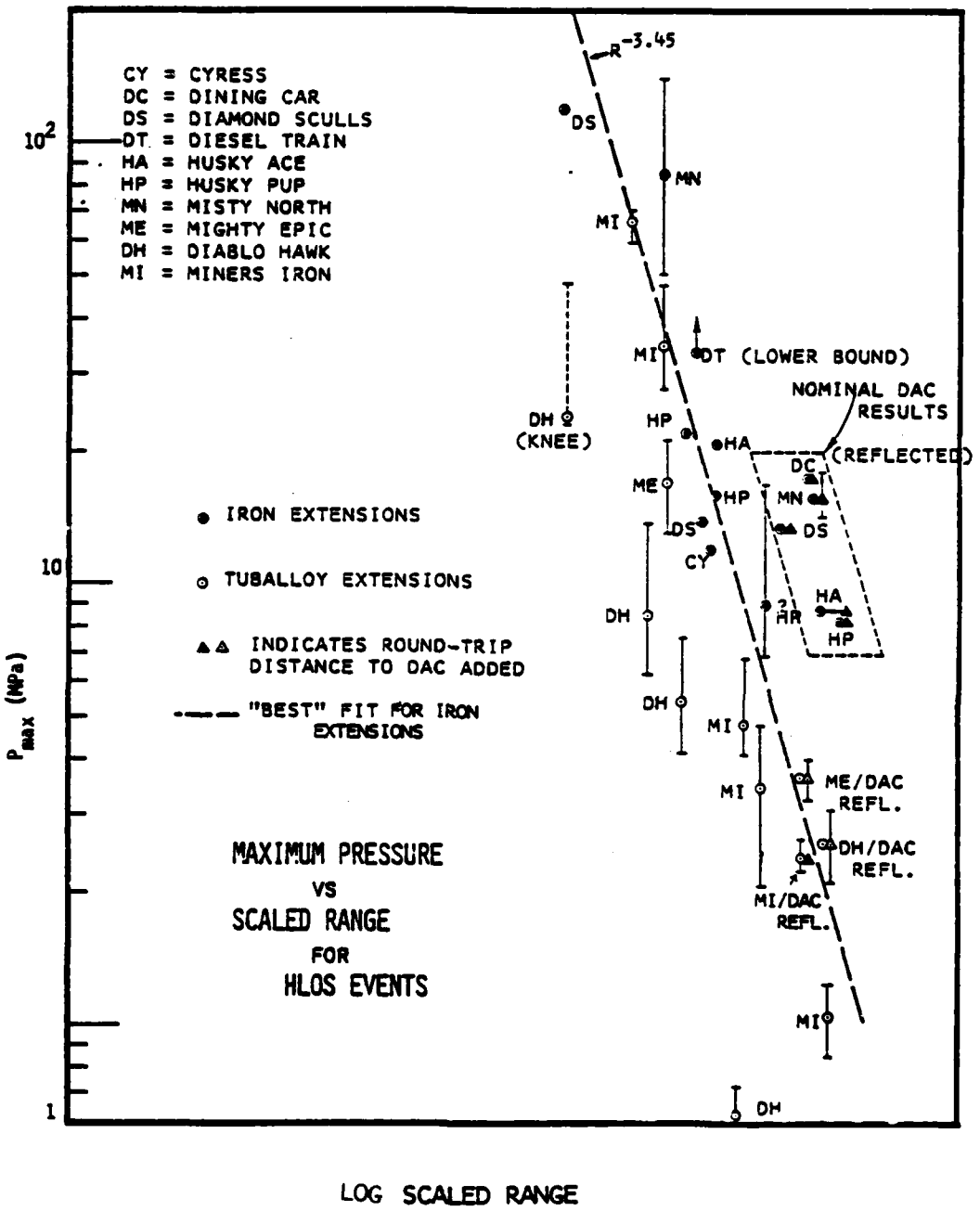

Figure 4.7. Maximum pressure vs. scaled range for HLOS events.

The next improvement planned for closure design is the helical wrap. Analysis of laboratory simulation of its performance (see discussion in Ref. (1) and summary in Section 3) indicates that it reduces target damage by deflecting or intercepting the jetting particulates. It is currently thought (by us at least) that the helix performs this function by being turned into the path of the particulates by the faster-arriving vapor flow. Because of this apparent need for some vapor flow and the strong possibility that cratering (particulate) flow is a greater threat to experiments and containment hardware than the vapor flows currently experienced, it may not be fruitful to try to effect drastic further reduction of vapor injection by extension design. It may even be necessary to consider making the helix of lower density material when large pipe tapers are used, to enable it to turn into the stream quickly enough (note results obtained in PI's LS-5, Ref (2d).

The next improvement following the helical wrap may be an economical modification of the FAC concept. Some preliminary thinking was done during the contract period on the use of a conical device that is given a modest initial explosive-induced motion toward axis. The explosive could be detonated by prompt radiation, eliminating detonation initiation devices entirely. LOS plasma would be relied on to complete the closure. The plasma would move mostly into the space opened around the cone by the HE detonation and should ultimately make the closure tight. The fact that some of the already-modest LOS plasma energy might get past the closure is not considered significant. Experience with PI simulations, indicating that jetting particulates move preferentially along the pipe walls, suggests that such a device could intercept nearly all of the particulates even if not fully closed when they arrive. Such a device offers the possibility of many economies. For example, it appears capable of doing the muffler's job even better; it could work in conjunction with a helical wrap but could also replace it; and, most importantly, it could possibly even allow at least one of the MACs/DACs to be eliminated. More detailed analysis and calculations relating to this concept are being carried out as part of the follow-on research effort. The central

problem appears to be the need to insure that the plasma will not cause such energetic collapse of this configuration that particulate jetting is initiated. This would merely transfer the jetting problem from its present location to a more remote location. This requirement also implies that such a closure must be sufficiently far from the source that ground shock-driven pipe collapse beyond the closure is not a source of particulate jetting. This may require that it be located about 30 m or more from the source.

The selection of stemming materials has also received consideration. The Huron King experience stimulated reconsideration of the use of dry sand stemming along some part of the LOS because its high air void content results in rapid attenuation of the ground shock. This is the subject of a STREAK calculational study begun during the contract period. The two configurations compared were Miners Iron as-built and with sand stemming replacing the grout beginning 1 m beyond the end wall. Several cost-saving approximations were used: a plugged LOS out to the end wall; simplification of the material representation in the zero room; and omission of radiation transport. These are not thought to affect the questions of interest in any significant way. These calculations are part of the study mentioned above under extension-optimization. The 1 m offset was selected because of results obtained with an earlier RAD9 calculation. RAD9 showed an initially more rapid energy injection into the LOS, during the first 1 m of ground shock propagation, because of the delay in closing the extension. The subsequent energy injection rate was lower than with grout because of the weaker shock in the sand. The calculations did not get far enough in time during the contract period to allow firm conclusions (120 μs); however, the results indicate that there may be some significant (but not dramatic) reductions in LOS energy to be realized from optimization of the stemming materials. The results will be reported in detail when the study is completed.

Closure optimization may be entering a stage of rapid development. There is obviously the potential for great improvement in closure performance and substantial cost reduction. New concepts are being tried and

others are in conceptual development. The key role of both simulation experiments and calculational analysis in the evolution of concepts is obvious. We anticipate rapid progress in this area in the current research effort.

SECTION 5
RESIDUAL STRESS STUDIES

5.1 SRI GROUT SPHERES

SRI International has since 1976 been conducting small scale laboratory experiments to study the residual stress fields around explosively formed cavities in 12 inch diameter spheres of rock-matching grout. S-CUBED has been conducting finite difference simulations of the high explosive detonation and the subsequent non-linear dynamic processes which result in the formation of compressive residual stress fields in the grout surrounding the explosive cavity in order to validate our capability to calculate containment related phenomena. Before 1981 the only laboratory data available to be directly compared to the dynamic calculations consisted of final cavity radius and the pressure and integrated impulse at a quartz gauge emplaced in the bottom of the water tank surrounding the grout sphere. In 1981, SRI began to emplace particle velocity gauges inside the grout spheres. These consisted of concentric current-carrying loops of wire in a magnetic field cast symmetrically about the explosive charge. Here we discuss the constitutive modeling advances made to date to best simulate the particle velocity records in 2C4 grout.

Earlier work by Rimer and Lie, Reference (6), had shown that increases in strength above the static failure surface measured in the laboratory were necessary to match the measured cavity radius. These increases in strength were assumed to be proportional to the logarithm of strain rate experienced by a grout element. Strain rates of 10^5 - 10^7 s^{-1} were calculated at the shock wave for these small scale experiments so that the increases in strength were quite large. The calculations with strain-rate-dependent strength gave residual stress peaks of almost 1.0 Kbar, much greater than the 0.40 - 0.45 Kbar fracture initiation pressures measured by hydrofracturing from the explosively formed cavity.

Comparisons made between the measured particle velocity records and those calculated using the above models showed two major differences; the calculated positive velocity pulses were somewhat narrower than the measurements and the negative pulses were a factor of three too narrow. An extensive effort was initiated to improve the constitutive models, and, in particular, to widen the negative velocity pulse (the cavity rebound phase of the phenomenology) so important to the calculation of compressive residual stress fields. The constitutive modeling variations examined in 1981 are discussed beginning with the earliest changes and ending with the most up to date.

1. Crush curve variations: These mainly impacted the peak velocities at the largest ranges where void crushup is incomplete.

2. Shock damaged shear modulus: A decrease in shear modulus of a factor of almost three during loading resulted in larger peak particle velocities (in worse agreement with the measurements), slightly wider positive velocity pulses, and approximately 50 percent wider negative velocity pulses.

3. Shock damaged failure surface: The failure surface used for previous work was based on measurements of stress differences at confining pressures of 4 Kb. A calculation was made in which the allowable stress difference after shock loading was decreased 40% . This was based on laboratory material properties measurements made at TerraTek. Strain rate dependence was assumed to increase the strength of damaged grout in a similar manner to undisturbed grout. The shock damaged failure surface resulted in positive particle velocity pulses wider than the measurements, peak velocities larger than the data, an 18% reduction in calculated peak residual hoop stress and a slightly larger cavity. Not much improvement in negative velocity pulse width was achieved. On the whole however, the concept of a damaged failure surface appeared to be an improvement in the constitutive model.

4. P-V EOS and elastic moduli of grout: These variations gave second order changes in results at most.

5. Strength, strain rate dependence, and EOS changes in the models for the lucite shell surrounding explosive: These variations gave only second order changes in results.

6. HE-detonated or burned: At ranges greater than 1 cm, almost no changes in results from the full HE detonation calculation occurred when the HE was assumed to burn at constant volume and then to follow the JWL equation of state isentrope down in pressure from the initial volume.

7. Modified JWL constants for PETN explosive: Changes in the equation of state of the PETN explosive (density = 1.0 gm/cc) that did not alter the measured Chapman-Jouget pressure, detonation velocity and explosive energy were investigated. Some reduction in peak particle velocities was achieved at the velocity gauge locations inside 2.0 cm.

Based on the above constitutive modeling variations, particularly those which improved the calculational results significantly, i.e., changes (2) and (3), we hypothesized that a weakened central core of grout was needed to give the desired wide negative velocity pulses. All of the following modeling variations were directed toward that objective.

8. No strain rate strength dependence for damaged grout: This further reduction in the strength of the shock damaged grout (from (3)) resulted in higher peak velocities and wider positive velocity pulses, both of which were unsatisfactory, but widened the negative pulses significantly.

9. Other variations which either enlarged the damaged central core or increased the amount of damage beyond that measured in the laboratory widened the negative velocity pulses significantly but also widened the positive pulses as well.

10. Plastic work effects: The above results indicated that the grout remained strong during shock loading and only decreased in strength later. If true, this would result in a sufficiently narrow positive velocity pulse and a wide negative pulse. As a first try, the strain rate dependence on strength was made a function of the magnitude of the plastic work in a grout element, more plastic work resulting in a gradually lower dependence of strength upon strain rate. At some prescribed value of plastic work, no strain rate dependence was allowed for the damaged grout. This gave a 50 percent increase in negative pulse width compared to the results with standard strain rate dependence and shock damage.

11. Time dependent damage: In this model, the undamaged (intact grout) failure surface was assumed to be strain rate dependent while the damaged failure surface was given no strain rate dependence. A time dependent (Maxwell solid) relaxation of deviatoric stresses from the undamaged to the damaged failure surface was assumed to occur in a relaxation time dependent upon the amount of damage. This model has given the best results to date, i.e., correct peak velocities and positive velocity pulses, and negative velocity pulses only slightly narrower than the measurements. At years end, this constitutive model was being pursued further with excellent prospects for a successful simulation of the velocity data.

5.2 SANDIA HE TESTS IN G-TUNNEL TUFF

Sandia National Laborabories have been conducting high explosive tests in tunnel bed 5 of G-tunnel, Area 12, at NTS. Radial stresses at several ranges from the explosive and cavity pressure have been measured out to times of many hours as an experimental test of the

residual stress concept. The largest of these tests, Puff Too, described by Smith, Reference (7), used 1000 lb of TNT explosive. Stress vs time data for comparison with dynamic calculations was obtained from Puff Too as well as from two smaller 64 lb tests, RS11 and RS15. We have conducted finite difference simulations of these tests to improve our understanding of constitutive models for tuff.

The Sandia stress measurements showed a considerable scatter from test to test as expected for an earth material as variable as the saturated tuff. However, several features of the experimental results were quite interesting. The 1000 lb event gave an average cavity radius of 108 cm, which could easily be calculated with our constitutive models. However, the 64 lb tests gave a significantly smaller cavity (approximately 82 cm when yield scaled to 1000 lb). Calculations showed that more than 65% of the difference in scaled cavity radius could be explained by using the same failure strength for both if a strain rate dependent strength model was invoked. Strain rate dependent strength increases had already been used to explain the small cavity radii measured in SRI laboratory tests in grout and in tuff. A smaller scale test would have higher strain rates than a larger test and therefore a higher strength and smaller cavity.

Another feature of interest was the width of a dip in the stress vs time measurements seen both in RS11 and RS15. This dip has been correlated through numerical simulations with the width of the negative velocity pulse, i.e., with the duration of the cavity rebound. A calculation was made introducing a damage dependent decrease in shear modulus to widen the negative velocity pulse which also improved the calculated width of this dip in the stress record. When the velocity records from ther SRI grout spheres tests are successfully simulated, calculations of the Sandia tuff tests made with these constitutive models can be expected to widen the stress dip as well.

5.3 RESIDUAL STRESS RELAXATION

A central concern of the DNA containment program over the last year or so has been to build on the earlier work which demonstrated the existence of a residual stress field and determined how that field may change in time. The SRI work has clearly demonstrated that if hydrofracture of an exploded grout sphere is delayed for a period of many minutes, the measured hydrofracture pressure becomes comparable to that for an unexploded sphere. In other words, a residual stress has relaxed away by some process or other. A similar conclusion can be drawn from hydrofrac experiments at NTS where no evidence of a residual stress field around a former nuclear test can be found some months after the experiment.

Two mechanisms for stress relaxation have been suggested; one involves material creep, the other pore fluid migration. We made a number of calculations several years ago with a very simple effective stress law which assumed that the pore pressure was equal to the mean stress for fully saturated materials. Under these circumstances, the residual stress was calculated to relax away on a time scale governed by the permeability of the material and the viscosity of water. However, more elaborate effective stress models have been developed for elastic materials. We have attemped to incorporate these representations in order to do a "better" job of representing the physical situation.

In order to make progress, it is necessary to determine a number of material moduli which deal with drained and undrained materials. These moduli are not determined in the conventional suite of measurements made at TerraTek, so an experimental program was undertaken to determine the needed values. Unfortunately the time scale for the attainment of drained-material equilibrium was found to be very long, and there is serious question about the reliability of the experimental determinations. Nevertheless, a series of stress relaxation calculations was made with the best estimates of material moduli

for 2C4 grout. As a result the calculated residual stress relaxation would reduce the peak compressive stress around an explosive cavity by only about 15% . This value is disappointingly small compared to the 100% relaxation determined by the simpler model and apparently required by experiment.

At the present time further investigation is underway to determine the best effective stress law treatment. The relatively simple model previously used can be questioned for elastic materials. The full elastic treatment can also be questioned because there is reason to believe that material damage which would be particularly severe near the explosive cavity would significantly modify material properties and bring into question the applicability of an elastic treatment for that material. More definitive results are anticipated within the next reporting period.

5.4 MISCELLANEOUS ACTIVITIES

We have maintained a very active interest in many aspects of the grout spheres program through the years. As a result a number of analyses of the available data have been made, and suggestions for additional work have been made. These will be summarized very briefly below.

- There was some question concerning the reliability of the first set of decoupled tests made last year. Data from these experiments was carefully analyzed, and it appeared very likely that the precast cavities were filled with water before the explosive charge was fired. The experimental technique has been modified and the experiments redone successfully.

- An overall evaluation of the contribution of this work has been prepared for the COR in which the demonstration of the existence of the residual stress field and its relaxation in rock-type materials has been emphasized.

- We have contributed to periodic reviews of the grout sphere program.

- An experiment was suggested in which the explosive charge would be fired in a small, closed metal vessel. This was proposed as a technique to assure that all aspects of the experimental apparatus performed as expected. This experiment has been conducted successfully.

- Since two different mechanisms have been suggested to explain the observed residual stress relaxation, it seemed appropriate to suggest experiments which could choose between the mechanisms. The most straightforward possibility would involve experiments on dry material where pore fluid diffusion is not involved. To this end suggestions were made which might be suitable for the preparation of a dry alluvium-like material. In addition, other experiments were devised which could have shown the influence of creep and pore fluid diffusion, but the one dimensional beam geometry suggested was far from that of immediate concern in the containment program.

SECTION 6
MISCELLANEOUS

A number of tasks were undertaken during the year which do not fall well within the topics discussed above. They will be grouped together here.

6.1 KRAK MODELING ASSISTANCE

The KRAK code has been used at LANL to investigate fracture propagation from a borehole. Because the Sneddon crack shape formalism is used by that code, some approximation must be made to the pressure distribution from the origin to the cylindrical cavity wall in order to perform the Sneddon numerical integration. It is desirable to optimize the pressure distribution assumption so that the crack shape calculated by the Sneddon integral agrees as closely as possible with the "correct" shape as determined by finite element calculations for the real geometry being considered and making use of the pressure distribution thought to exist on crack surfaces. The following discussion describes the work done. First is a treatment of the analytical and numerical solution to the Sneddon problem. This is followed by a discussion of the finite element calculations of the expected crack shape in the vicinity of a pressurized borehole and finally, the recommended numerical algorithm to be used in KRAK to reproduce the finite element solution.

6.1.1. Analytical Crack Width Calculation

As part of the effort to provide an improved algorithm for crack width calculations in KRAK, several analytical crack width calculations were done using the LANL pressure distribution inside the crack and the Sneddon formalism. In an infinite elastic medium the crack width can be represented by integrals of the pressure distribution along the crack wall.

Four different cases were considered:

CASE I: Linear crack of length L. This is expected to be a good approximation when the length of crack is short compared to the cavity size. Assuming plane strain conditions, the half width of the crack at the position x along the crack is given by

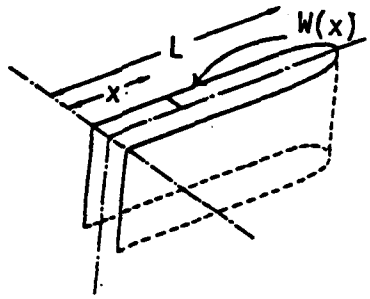

$$W(x) = \frac{2(1-\nu)L}{\pi G} \int_{f_x}^{1} \frac{f_2\, df_2}{\sqrt{f_2^2 - f_x^2}} \int_{0}^{f_2} \frac{p(f_1)df_1}{\sqrt{f_2^2 - f_1^2}}$$

where $f_x = \frac{x}{L}$

In the above equation G and ν represent the shear modulus and Poisson's ratio of the material and p(x) represents the pressure distribution along the crack.

CASE II: Penny shaped crack with the radius equal to the crack length L. The half crack width at the distance r from the axis is given by

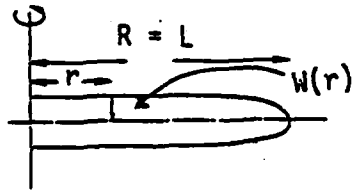

$$W(r) = \frac{2(1-\nu)\, R}{\pi G} \int_{f_r}^{1} \frac{df_2}{\sqrt{f_2^2 - f_r^2}} \int_{0}^{f_2} \frac{f_1 p(f_1)\, df_1}{\sqrt{f_2^2 - f_1^2}}$$

where R = L and $f_r = \frac{r}{R}$.

CASE III: Large penny shaped crack with the cavity region at the origin without cavity pressure. The half crack width is given by

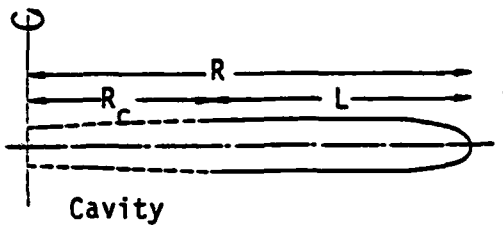

$$W(r) = \frac{2(1-\nu)R}{\pi G} \int_{f_r}^{1} \frac{df_2}{\sqrt{f_2^2 - f_r^2}} \int_{f_{R_C}}^{f_2} \frac{f_1 p(f_1)\, df_1}{\sqrt{f_2^2 - f_1^2}}$$

where $R - R_c = L$. $f_r = \frac{r}{R}$ and $f_{R_C} = \frac{R_c}{R}$.

In the above equations, R_c represents the cavity radius.

CASE IV: Same as CASE III with the cavity pressure applied in the cavity region. The integral expression for CASE II can be directly used with $R = R_c + L$.

For the numerical integration the pressure was assumed to vary linearly within each cell, i.e., in the i-th cell with p_i and $f_i = \left(\frac{r_i}{R} \text{ or } \frac{x_i}{L}\right)$ given at the left and p_{i+1} and f_{i+1} given at the right boundary of cell,

$$p(f) = a_i + b_i\, f \text{ for } f_i \le f \le f_{i+1}$$

where

$$a_i = p_i - \frac{p_{i+1} - p_i}{f_{i+1} - f_i} f_i$$

$$b_i = \frac{p_{i+1} - p_i}{f_{i+1} - f_i}$$

Using this approximation the evaluation of the first integrals at the J-th point becomes the sum of the following integrals

$$\alpha_i \int_{f_i}^{f_{i+1}} \frac{df}{\sqrt{f_J^2 - f^2}}, \quad \beta_i \int_{f_i}^{f_{i+1}} \frac{f\, df}{\sqrt{f_J^2 - f^2}}, \text{ and } \gamma_i \int_{f_i}^{f_{j+1}} \frac{f^2\, df}{\sqrt{f_J^2 - f^2}}$$

from i = 1 to J - 1

where α_i's, β_i's, and γ_i's are constant within each cell. These elementary integrals can be easily evaluated. After the first of the double integrals is evaluated at each discrete point, these integrals are again assumed to vary linearly within each cell. Following the same procedure the second integral at the K-th point can be approximated by the sum of the following integrals,

$$\alpha_i \int_{f_i}^{f_{i+1}} \frac{df}{\sqrt{f^2 - f_K^2}}, \quad \beta_i \int_{f_i}^{f_{i+1}} \frac{f\,df}{\sqrt{f^2 - f_K^2}}, \quad \text{and} \quad \gamma_i \int_{f_o}^{f_{j+1}} \frac{f^2\,df}{\sqrt{f^2 - f_K^2}}$$

from $i = K$ to $I_{max} - 1$

where α_i's, γ_i's and γ_i's are constant within each cell.

The results of crack width calculations using the LANL pressure distribution for the four cases are shown in Figure 6.1. It is clear that the initial LANL result corresponded to Case II which ignored the presence of the borehole and assumed the crack simply translated to the axis. It is also clear that other assumptions about how to solve the Sneddon problem in this real-world case lead to very different estimates of crack width for a given pressure distribution. However, the crack width influences flow into the crack, the crack length, and the pressure distribution, so it is important to use the best approximation available for the crack width formalism.

6.1.2. Simple Algorithm for Crack Width Calculation

The next step was to determine the "correct" crack width for the actual geometry under investigation by making finite element calculations. This provided a standard of comparison for the algorithms to be developed. Figure 6.2 shows the crack width calculated for a 5.9 cm long crack extending out from a cylindrical cavity of 7.5 cm radius and 60 cm length. The LANL-supplied pressure distribution was used in the crack.

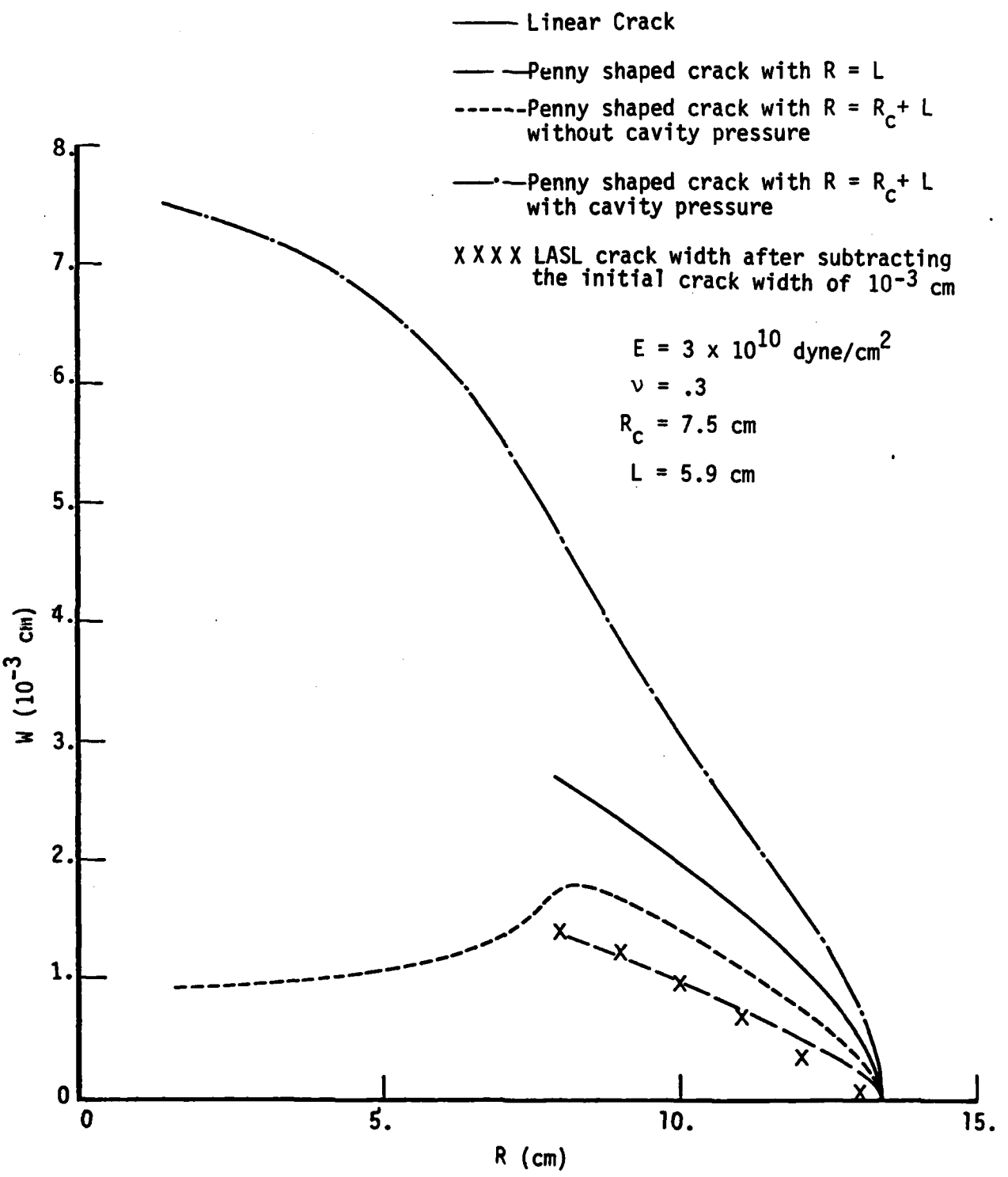

Figure 6.1. Crack width comparison for LASL Pressure Distribution.

FIGURE 6.2. Comparison of Calculated Crack Widths for Different Pressure Distributions in Cavity

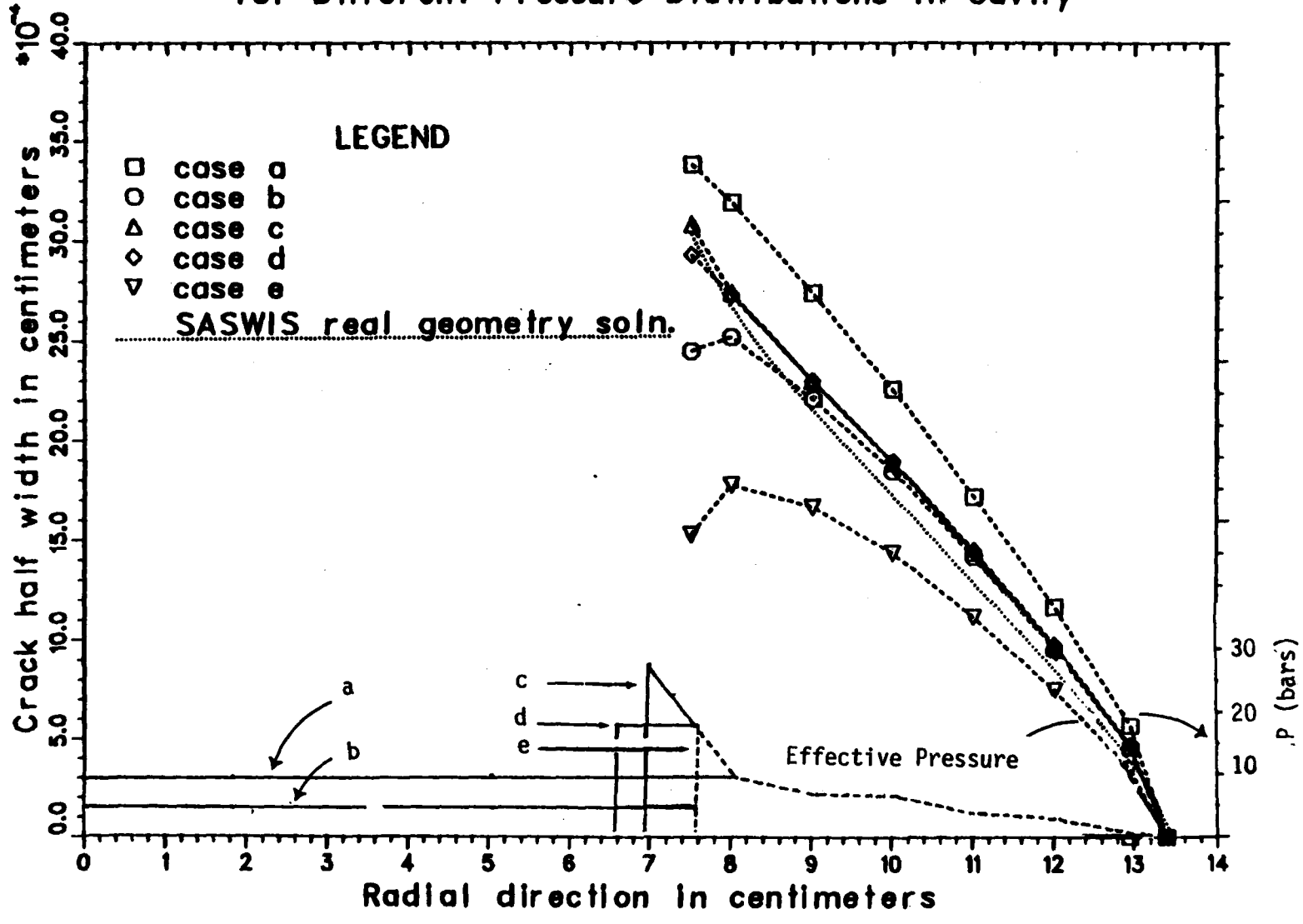

For comparison, the several different pressure distributions shown in Figure 6.2 were also used in Sneddon calculations to determine the various shapes shown in the figure. The simple expedient of extrapolating the pressure profile 0.6 cm into the borehole (c), or extending the cavity pressure 1 cm into the borehole (d) give good agreement with the correct crack shape within the uncertainty of the finite element method.

The question next arises as to how the approximate algorithms work for longer cracks. This was investigated by simply stretching out the LANL pressure distribution to crack lengths of 29.5 and 59 cm. Figure 6.3 shows a comparison of several analytic crack width results with the "correct" finite element solution. In this and the following figures the "pressure fix" referred to in the legend means that the cavity pressure was assumed to act on 1 cm of the borehole at the cavity wall as in profile d of Figure 6.2. Figure 6.4 shows similar results for a 59 cm long crack.

Figure 6.5 demonstrates the relative importance of cavity influence for the different crack lengths. The ratio of the crack width at the opening for the case of cavity pressure applied to that for the case without cavity pressure applied and the ratio of the crack opening of real case to that of penny shaped crack without cavity pressure are shown for the three different crack lengths. The ratio of the real crack width to the width calculated with the cavity pressure in 1 cm of the cavity is also shown in this figure.

These results demonstrate that the simple scheme of loading the cavity pressure in 1 cm of the crack adjacent to the opening of a penny shaped crack leads to analytic results which approximate the correct shape quite well even for cracks 5 to 10 times longer than those actually calculated by LANL. This suggests a simple calculational procedure to be used in KRAK to calculate crack openings from this particular cylindrical borehole geometry.

FIGURE 6.3 Comparison of Calculated Crack Widths for Different Geometry Cases (29.5 cm. crack)

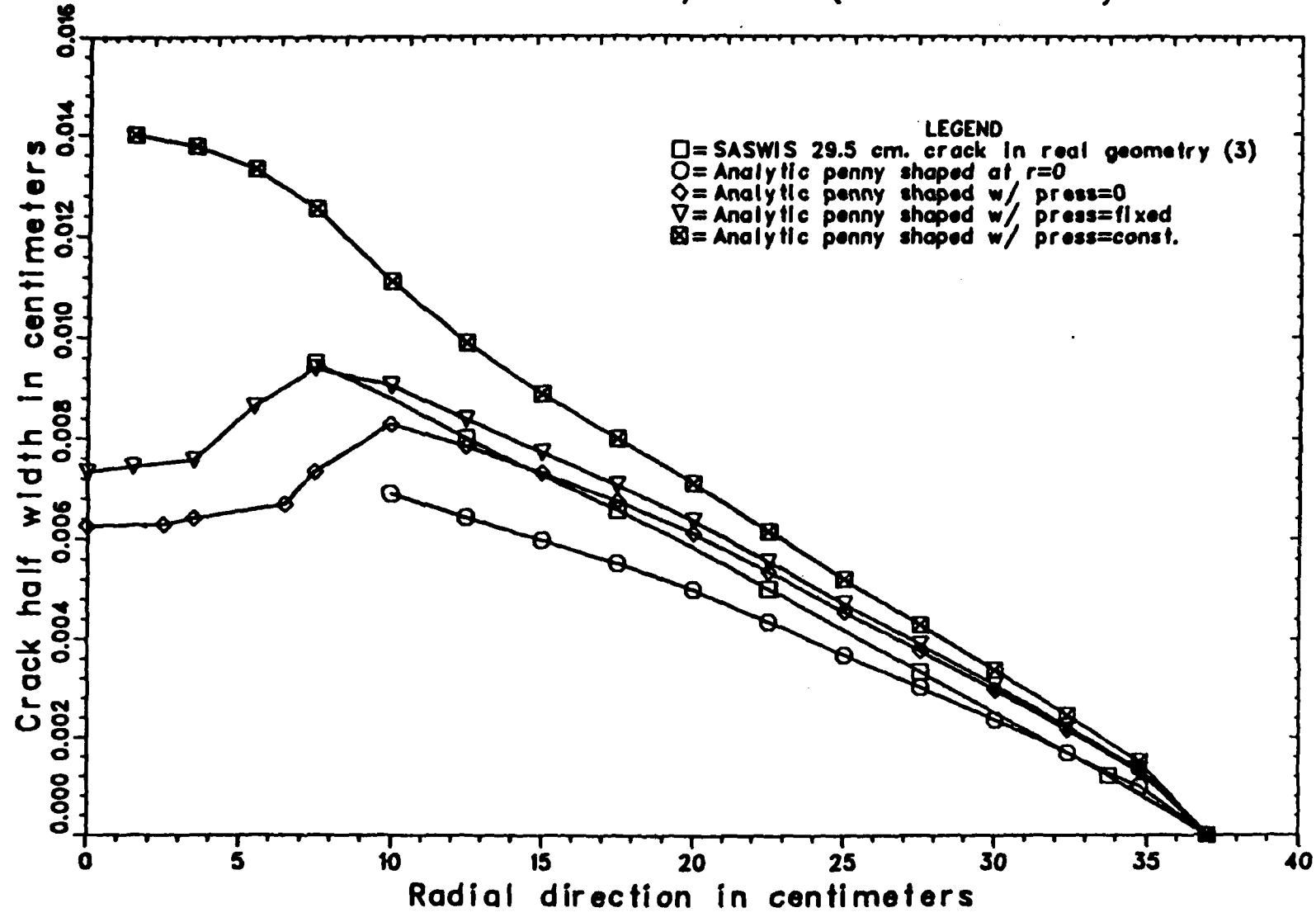

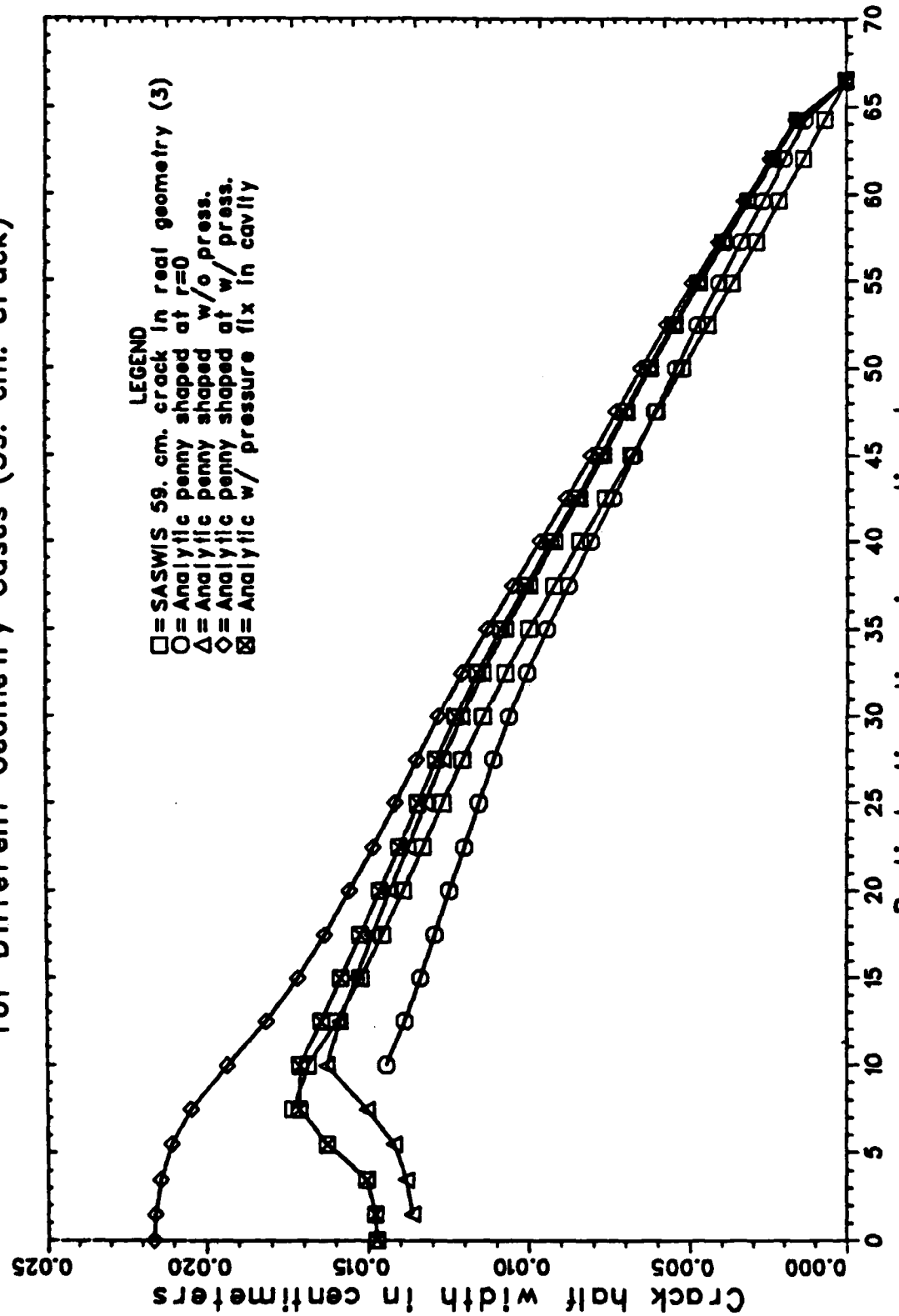
Comparison of Calculated Crack Widths
for Different Geometry Cases (59. cm. crack)
LEGEND
□= SASWIS 59. cm. crack in real geometry (3)
○= Analytic penny shaped at r=0
△= Analytic penny shaped w/o press.
◇= Analytic penny shaped at w/ press.
⊠= Analytic w/ pressure fix in cavity
Crack half width in centimeters
0.000
0.005
0.010
0.015
0.020
0.025
Radial direction in centimeters
0
5
10
15
20
25
30
35
40
45
50
55
60
65
70

FIGURE 6.4.

FIGURE 6.5. Cavity Influence as a Function of Crack Opening

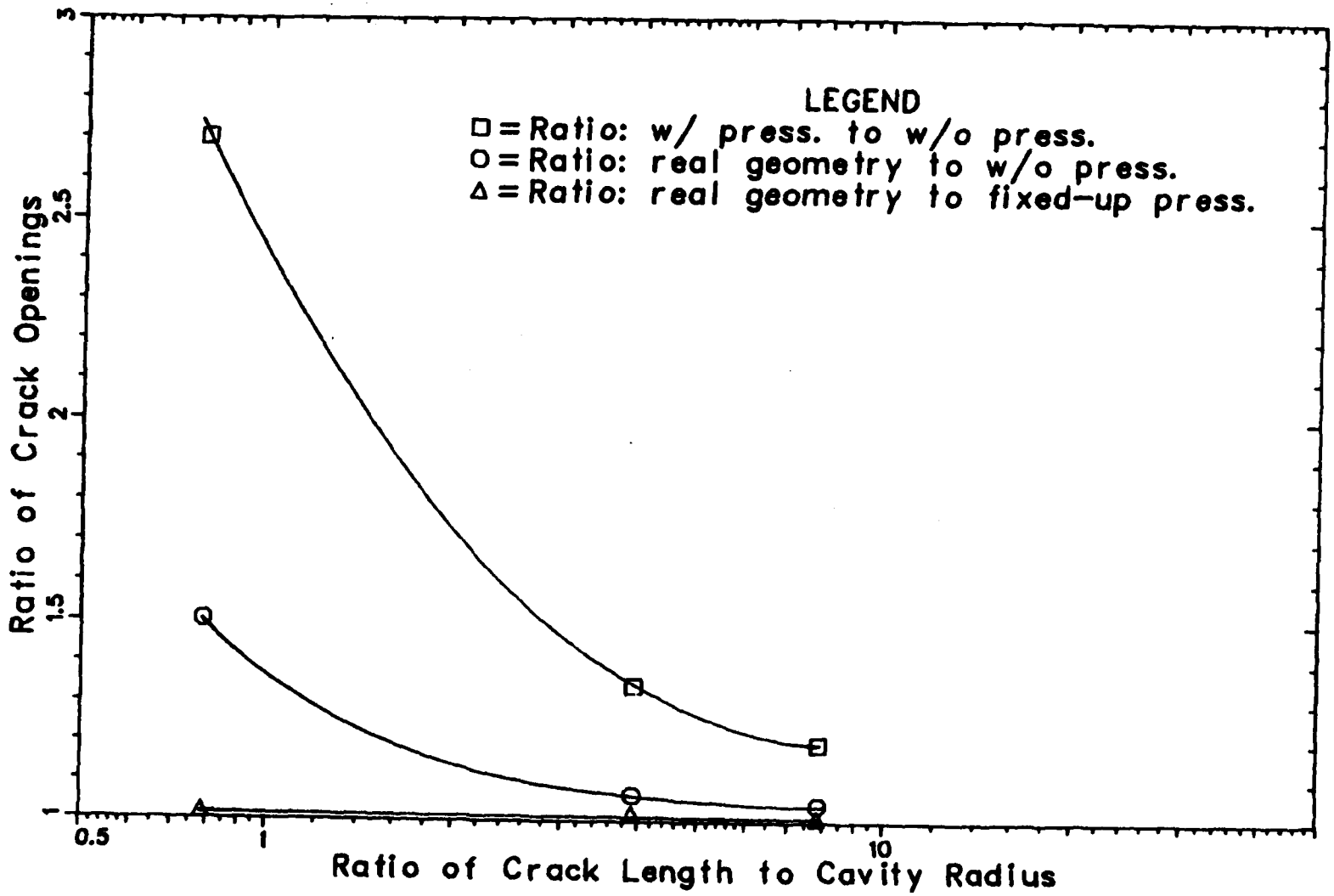

This calculated algorithm was developed for this particular geometry. There is no reason to expect it to apply to any other problem such as a crack propagating from a spherical cavity. The whole process of comparing finite element results and analytic approximations including various treatments of the cavity region must be repeated in order to find an appropriate algorithm for a different problem.

6.2 CONTAINMENT SYMPOSIUM

S-CUBED personnel presented three papers at the Containment Symposium held at the Naval Post-Graduate school, Monterey, California, August 26-28, 1981. These papers are:

"Medium Property Effects on Containment" - Norton Rimer
"The Nature of LOS Pipe Flow" - J. R. Barthel
"Evaluation of Red Hot" - Russell E. Duff

These three documents will appear in the Proceedings of the Symposium.

6.3 CEP PARTICIPATION

A member of the S-CUBED Staff has continued to serve as a consultant member to the Department of Energy Containment Evaluation Panel. This organization reviews and comments on the plans for all underground nuclear tests to be conducted by the United States. This involvement has represented a relatively minor but continuing expenditure of contract resources.

REFERENCES

1. Barthel, J.R., and Wiehe, J. W., "Analysis of Jetting Simulation Experiments", Technical Report DNA-TR-81-30 (also S-CUBED Report SSS-R-81-4898), 1 July 1981.

2. "Asymmetric Collapse of LOS Pipe", (A series of Physics International Reports all bearing same title):
   (2a) Moore, E.T. Jr., and Funston, R. (LS-2), DNA 5023F, July 1979.
   (2b) Moore, E.T. Jr., and Funston, R. (LS-3), DNA 5022F, May 1980.
   (2c) Mumma, D., Thomsen, J., Funston, R., and Moore, E.T. Jr., (LS-4) PIFR-1403, March 1982.
   (2d) Mumma, D., Thomsen, J., Funston, R., and Moore, E.T. Jr., (LS-5) PIFR-1517, March 1982.

3. Birkhoff, McDougall, Pugh, and Taylor, Journal of Applied Physics, 19, p 563, 1948.

4. Birkhoff, G. and Zarantonello, E.H., "Jets, Wakes and Cavities", Academic Press, 1957.

5. Barthel, J. R., Peyton, S., Pyatt, K. D., and Wu, H. E., "Ablation and Boundary Layer Growth Effects Behind High Speed Shock Waves in Pipes and Tunnels", DNA5388F (also S-CUBED report SSS-R-80-4521), July 1980.

6. Rimer, N. and Lie, K., "Spherically Symmetric Calculations of the SRI Grout Spheres Experiments for Four Different Laboratory Configurations", S-CUBED Topical Report SSS-R-80-4240, Submitted to DNA November 1979.

7. Smith, C. W., "Puff Too: A Residual Stress Experiment", Sandia Laboratories Report SAND79-1674, 1979.

DISTRIBUTION LIST

DEPARTMENT OF DEFENSE

Defense Nuclear Agency
ATTN: SPTD, T. Kennedy
4 cy ATTN: TITL

Defense Technical Information Center
12 cy ATTN: DD

Field Command
Defense Nuclear Agency
ATTN: FCT, COL G. Ballantine
ATTN: FCTT, G. Ganong
ATTN: FCTT, W. Summa
3 cy ATTN: FCTK, B. Ristvet
3 cy ATTN: FCTK, C. Keller

DEPARTMENT OF ENERGY

Department of Energy
Nevada Operations Office
ATTN: R. Newman

OTHER GOVERNMENT AGENCY

Department of the Interior
US Geological Survey
ATTN: R. Carroll
ATTN: A. Fernald

DEPARTMENT OF ENERGY CONTRACTORS

Desert Research Institute
ATTN: D. Schulke Sec Off for C. Case
ATTN: D. Schulke Sec Off for P. Penske

University of California
Lawrence Livermore National Lab
ATTN: L. Makague
ATTN: F. Morrison
ATTN: R. Terhune
ATTN: B. Hudson
ATTN: L-209, G. Higgins

DEPARTMENT OF ENERGY CONTRACTORS (Continued)

Los Alamos National Laboratory
ATTN: T. Kunkle, ESS-5
ATTN: F. App
ATTN: C. Keller
ATTN: B. Travis
ATTN: R. Brownlee

Sandia National Lab
ATTN: Org 7112, C. Mehl
ATTN: C. Smith

DEPARTMENT OF DEFENSE CONTRACTORS

California Research & Technology, Inc
ATTN: M. Rosenblatt

Kaman Tempo
ATTN: DASIAC

Pacific-Sierra Research Corp
ATTN: H. Brode, Chairman SAGE

Pacifica Technology
ATTN: D. Patch

Physics International Co
ATTN: D. Mumma
ATTN: E. Moore

R&D Associates
ATTN: P. Haas

S-CUBED
ATTN: R. Duff
2 cy ATTN: J. Bartel
2 cy ATTN: W. Proffer
2 cy ATTN: K. Lie
2 cy ATTN: N. Rimer
ATTN: C. Dismukes

SRI International
ATTN: A. Florence